2016

Effect of Poisson's Ratio on Material Properties Characterization by Nanoindentation with a Cylindrical Flat Tip Indenter

MD Mehadi Hassan
mdmehadi.hassan@jacks.sdstate.edu

EFFECT OF POISSON'S RATIO ON MATERIAL PROPERTIES CHARACTERIZATION BY NANOINDENTATION WITH A CYLINDRICAL FLAT TIP INDENTER

BY

MD MEHADI HASSAN

A thesis submitted in partial fulfillment of the requirements for the

Master of Science

Major in Mechanical Engineering

South Dakota State University

2016

EFFECT OF POISSON'S RATIO ON MATERIAL PROPERTIES CHARACTERIZATION BY NANOINDENTATION WITH A CYLINDRICAL FLAT TIP INDENTER

This thesis is approved as a creditable and independent investigation by a candidate for the Master of Science in Mechanical Engineering degree and is acceptable for meeting the thesis requirements for this degree. Acceptance of this does not imply that the conclusions reached by the candidates are necessarily the conclusions of the major department.

Dr. Zhong Hu, Ph.D.
Thesis Advisor Date

Dr. Kurt Bassett, Ph.D.
Head, Department of Mechanical Engineering Date

Dean, Graduate School Date

ACKNOWLEDGEMENTS

Foremost, I would like to express my sincere gratitude to my thesis supervisor Professor Zhong Hu for continuous support of my graduate study and research, his guidance, knowledge and patience with me. His encouragement during my research and his willingness to investigate for the true results and understanding of the research problems has shown me how to work with integrity and tried to clear my confusions with an intellectual explanation. From the beginning of the research to the completion Dr. Hu has guided me and assisted me in appreciation of this topic.

Besides my advisor, I would like to thank Professor Todd Letcher for support me mentally and encourage me during my thesis work. I would like to thank my friends who proffered many consultation that were helpful for this work.

My sincere thanks goes to the graduate school of South Dakota State University and computational facility support from Brian Moore for allowing me to perform this research with ANSYS, Inc.

Finally, I am thankful to my parents for their financial support and encourage me to pursue my dreams and desire. Without their consent and guidance, I would not be able to be here.

CONTENTS

LIST OF FIGURES

LIST OF TABLES

ABSTRACT

EFFECT OF POISSON'S RATIO ON MATERIAL PROPERTIES CHARACTERIZATION BY NANOINDENTATION WITH A CYLINDRICAL FLAT TIP INDENTER

MD MEHADI HASSAN

2016

Nano indentation technology is commonly used to determine the mechanical properties of different kinds of engineering materials. The young's modulus of the materials can be calculated with the load depth data obtained from an indentation test with a known Poisson's ratio. In this investigation the NANOVEA micro/nano-indentation tester with a cylindrical flat-tip indenter will be used to find the elastic modulus, hardness and Pile up. Low carbon steel AISI1018, alloy steel AISI 4340 and aluminum alloy 6061 were selected for the case study. Finite element (FE) analysis using axisymmetric 3-D models used to establish the relationship between Poisson's ratio and the deformation of indentation / materials strain hardening exponential index with a cylindrical flat tip indenter. The modeling was done by considering the Poisson ratio ranging from 0 to 0.48 in order to find the influences of Poisson ratio on the elastic-plastic properties was verified by associated experimental results. From the modeling results, it was found the indentation depth has very little effect on calculating the elastic modulus of the sample material in the same Poisson ratio and the hardness slowly increases with the increase of maximum indentation depth as well as increase the Poisson ratio. The maximum pile up value for the three materials decreases with the decrease of Poisson ratio that was very sensitive.

Chapter 1 Introduction

1.1 Background

1.1.1 Poisson Effect

Advent technology in modern times has outstripped so many challenges in the material system world. Uncovering accurate mechanical properties such as Young's modulus, Poisson's ratio, yield strength, and ultimate strength have become critical factors for making research and design of engineering materials. Among all the materials properties, Poisson's ratio define as the negative ratio of transverse to axial strain, is one of the fundamental parameter whose accurate value would give more reliable and precision value for any design of structures where all dimensional changes resulting from the application of the applied force needed to be taken into account [1]. When a material is compressed in one direction, it usually tends to expand in the other two directions perpendicular to the direction of compression. This phenomenon is called the Poisson effect. In the early times, Poisson's ratio was characterized at macro level obtained from stress strain relationship by using tensile testing machines according to the American Society for Testing and Materials (ASTM) standard [1] [2]. This macro/nano-scale mechanical properties that are critical to characterize for advanced material system like thin films, coatings, nanostructured materials. During the last 20 years, researchers have become more interested in mechanical properties of small volumes of materials which may differ from macro scale properties due to the size and surface effect [3]. The resulting technique, termed nanoindentation, has become more ubiquitous for mechanical property measurements at surfaces.

1.1.2 Nanoindentation

Nano-indentation is widely adopted method to measure elastic, plastic and time dependent mechanical properties, including the hardness, Young's modulus, Poisson's ratio of thin films and structural applications of materials with micro or nano-sized features. This method has gained popularity with the development of machines that were capable of recording very small loads and displacements to a high level of precision and accuracy [4]. The size of the mechanical systems is decreasing day by day and especially will begin to approach atomic length scales. Thus it's obligatory to develop experimental methods and corresponding theoretical analysis to characterize material properties at these nano scales. In recent years new experimental and computational approaches are being inaugurate to interpret the experimentally observed phenomena with the veritable mechanical testing at small scales.

The depth sensing indentation with high tenacity of load and displacement up to nanoscale works on the principle, where an indenter with known geometry is penetrated into a sample material's surface up to a certain depth and then recant. Both the applied load and indentation depth is simultaneously monitored and recorded by high resolution sensors of the indentation system. If the material properties and the experimental indentation data is known then desired mechanical properties can be extracted [5].

1.1.3 Major mechanical properties

The mechanical properties of a material are those properties that involve a reaction to an applied load in the elastic or plastic behavior of a material under pressure. The most common mechanical properties are tensile strength, ductility, hardness, modulus of elasticity, yield strength impact resistance, fracture toughness and fatigue.

Elasticity is the ability of a material to return to its original shape after the load is removed whereas plastic properties refers to the ability of a material to deform permanently without breaking or rupturing. Hardness is the property of a material for indentation and scratching that measure how resistant of solid surface is to change of permanent shape when a compressive external force is applied. The yield strength is the minimum stress which produces permanent plastic deformation. Elastic modulus is defined as the slope of a stress-stain curve in the elastic deformation region which defines stiffness of a material as it undergoes stress to deform along an axis and then returns to its original shape after the force is removed. Ultimate yield strength is the maximum stress that a material can carry without the permanent change of dimensions and ultimate tensile strength is the maximum amount of tensile stress that a material can withstand before failing. Proportional limit is the highest stress at which stress is linearly proportional to strain. The elastic modulus can be easily determined by nanoindentation as need few analytical solution relating to the applied load, indentation depth. Moreover the plastic properties such as yield strength can hardly be found due to the finding of analytical solution.

1.2 Previous Work

Zheng et al. [6] performed indentation on articular cartilages for simultaneous estimation of Poisson's method and Young's modulus, in which they established the relationship between Poisson's ratio and the deformation-dependent indentation stiffness for different aspect ratio (indenter radius/tissue original thickness) in the indentation test after making computer-modeling using Finite Element analysis. From the FE results, they found that the indentation stiffness linearly increased with the deformation. Based on the deformation –dependent indentation stiffness obtained from the force-deformation data, they extracted value of Poisson's ratio and then calculated Young's modulus with the estimated Poisson's ratio. Their numerical results showed percentage errors of estimated Poisson's ratio and corresponding Young's modulus ranged from 1.7% - 3.2% and 3.0%-7.2% respectively, with the aspect ratio greater than one. Kim et al. [7] was measured the Poisson's ratio of MEMS thin film by designing double ring shaped specimen in which they analyzed the load –deflection data of double ring specimen subjected to nano-indenter loading. They obtained the Poisson's ratio by comparing the stiffness results of the double-ring specimen from the analytical model and the nano-indentation experiment which was measured to be 0.254 with deviation of 0.0125. They validate their results comparing with the Poisson's ratio of LPCVD polysilicon with the thickness 2.33 μm and demonstrated their method as reliable one.

Liu et al. [8] was determined Young's modulus and Poisson's ratio of coatings on the basis of Hertz theory for the contact of coated bodies by means of elastic indentation tests where they analyzed the load-displacement data from the spherical indentation. They determined these values at the same time through minimizing the differences

between the measured and specifically defined modified Young's moduli so that they didn't require to make any assumption on pressure distribution and Poisson's ratio.

Garcia and Rasty [9] obtained Poisson's ratio for bulk materials by using the non-linear least squares approach. They explored the Hertzian contact equation by not assuming a priori value of Poisson's ratio. Instead of assuming value for Poisson's ratio, they used least-squares approach emphasizing only the elastic portion of the Hertzian contact, and thus made simultaneous determination value of elasticity and Poisson's ratio.

Clifford et al [10] investigated the effect of the Poisson's ratios by using FEA for both the over layer and the substrate on the nanoindentation of an elastic two-phase system. They calculated the combined modulus as a function of indentation depth for a variety of different systems. They developed analytical equations to account change in Poisson's ratio for both layers and thus showed nanoindentation results may be expressed analytically using a simple extension of the equation of Clifford and Seah [11]. And that function can describe the reduced modulus value measured using Oliver and Pharr's method [12].

Jung et al [13] analyzed two different techniques to measure mechanical properties such as the elastic modulus and the residual stress of thin film, bulge test and nano-indentation test. In the bulge test, uniform pressure applies one side of thin film to measure the membrane deflection that allows characterization of the mechanical properties such as the elastic modulus and the residual stress. They modified King's model that can be used to estimate the mechanical properties of the thin film to avoid the

effect of substrates. Both techniques are different of the mathematical relationship between the modulus and Poisson's ratio.

Bamber et al [14] discuss two different techniques, nanoindentation and acoustic microscopy; both of which can be used to determine Young's modulus and Poisson's ratio. They involve the introduction of the gamma correction factor [15] which requite for the elastic–plastic contact in real materials and compared graphically experimental results of Young's modulus and Poisson's ratio by both techniques. The intersection of the acoustic curve and the nanoindentation curve for fused silica provided an accurate estimation of Young's modulus and Poisson's ratio.

Chen et al [16] studied the effect of Poisson's ratio on two-dimensional elastic-plastic stress by using the body force method which caused the plastic deformation due to force doublets.

Pintaude et al [17] discusses five model expand of the Tabor proposes, showing that their similarity depending on the specific mechanical properties of tested material which used to make the conversion between yield stress and hardness. They used diamond as a spherical indenter to avoid large deformations during the indentation process.

Green et al [18] showed the location of the maximum elastic distress both in spherical and cylindrical Hertzian contacts based on the maximum shear stress theories. It depends on Poisson ratio that the maximum distress can occur at the contact surface as well as underneath the surface. In the both case maxima of the von Mises and shear stresses occur at two different Poisson ratios 0.1938 and 0.24 accordingly.

Norbury et al [19] investigated the effect of Poisson's ratio on the deformation of auxetics behaviors of the material and other parameters including the sample thickness, indentation depth and indenter size. They conclude the negative Poisson's ratios have also the direct influence on the membrane deformation as the depth load curve, the deflection profile and the contact area.

Abd-Elhady et al [20] analyzed the influence of Poisson's ratio on stress and strain concentration factors of plate with circular notch by using three dimensional finite element method to determine the site of crack initiation. They conclude that the maximum stress and strain concentration factors increase with increasing the Poisson's ratio varied from 0.1 to 0.4 with decrease the biaxial ratio.

Yu et al [21] and Grant et al [22] investigated the influence of Poisson's ratio on the thickness-dependent stress concentration factor (SCF) of a plate with elliptic holes by use of three-dimensional finite element method. The result shows that the SCF increases with the increase of Poisson's ratio from 0.1 to 0.49.

Abdulaliyev et al [23] and J. Dundurs et al [24] described theoretically the effect of Poisson's ratio on three-dimensional stress distribution in plane elasticity. The stress elements are individualistic from Poisson's ratio with surface tractions of the body.

E. Liu et al [25] illustrated the viscoelastic-plastic behavior of viscoelastic materials in linear rheological constitutive model to obtain Poisson's ratio by load step indentation.

1.3 Motivation

Traditionally tensile test was the most popular method for measuring mechanical properties which is a devastating test and takes long time as need massive machine effort. This test is impracticable to perform on nano scale or area such as an area being laser scanned, explosive-bonded, thin film-coated or micro/nano-structured materials. In order to overcome these issues, nanoindentation techniques as a more reliable, cost effective, flexible and accurate method are widely used in a nano scale which is motivated by modern applications, e.g. microelectronics, MEMS, photovoltaic cells, laser treatment of surfaces, explosive bonding adhesion and coating of thin layers in complex structures etc.

In nanoindentation technique it is impossible to characterize mechanical properties without Poisson ratio of the specimen. In this case Poisson ratio is important factor to characterize material properties. The relationship between Poisson's ratio and stiffness obtained from the force-deformation data that extracted value of Poisson's ratio is needed to calculate the Young's modulus with the estimated Poisson's ratio.

Previously nanoindentation was concentrated on the Berkovich indenter tip, a pyramidal shape diamond tip or other indenter like spherical or conical indenters. But now a days the cylindrical flat tip indenter can be used, which has some attractive features such as constant contact area and leads to a faster and feasible way for finding mechanical properties of endless unknown material specimen within micro/nano-scale. Major motivation for this work is to overcome the issues related the effect of Poisson ratio on materials properties with the cylindrical flat tip indentation so that the benefits offered by this kind of indenter can be utilized.

1.4 Objectives

The purpose of this research is explore the relationship of Poisson's ratio and the deformation of indentation / materials strain hardening exponential index with cylindrical flat punch. More specifically the following concerns have been addressed in details:

- Develop a relation between Poisson ratio and the maximum pile up.
- Build a three dimensional solid model for AISI 1018, AISI 4340 and 6061T6 materials based on the true stress strain data and perform finite element simulation.
- Determine the load displacement curve for different value of Poisson's ratio of range (0-0.48) for three materials where keeping all other parameters constant.
- Validate the proposed FE model via evaluating the mechanical behavior of cylindrical flat tip nanoindentation with the results found from literature.
- Analysis mechanical properties including elastic modulus, hardness, pileup and compare the results with the experimental ones for three materials.
- Extraction of Poisson's ratio through micro/nano indentation testing with cylindrical flat tip indenter.

Chapter 2 Theory

2.1 Poisson's Ratio

Poisson's Ratio, ν is define as absolute value of the ratio of Transverse / Lateral strain to the longitudinal / axial strain in the elastic region. In other word the Poisson ratio is the fraction of expansion divided by the fraction of compression. Mathematically expressed as follows:

$$\nu = \frac{\epsilon_{\text{Transverse}}}{\epsilon_{\text{Longitudinal}}} = \frac{\Delta d}{D} \Big/ \frac{\Delta l}{L} \tag{2-1}$$

When a material undergo a tensile force P, it occurs a stress regarding to the applied force. In proportion to the stress, the cross section is declined by Δd from the diameter D and the length elongates by ΔL from the length L illustration in Fig. 2.1.

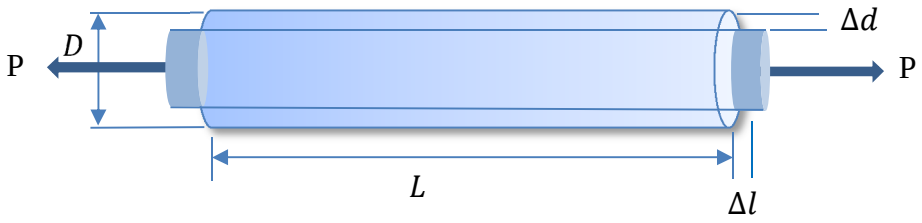

Fig. 2.1: Tensile test of a sample.

When a material is compressed in one direction, it usually tends to expand in the other two directions perpendicular to the direction of compression. This circumstance is called the Poisson effect.

2.2 Stress-strain correlation

Tensile test is most reliable test for the characterization of the materials property. Generally tensile test uses for large instrumentation which needs immense strength to pull apart metal and plastic. In the tensile test, load is applied on the sample that undergoes elastic deformation followed by plastic deformation. The sample will always return to its original dimensions in the elastic region. Further increasing the load it stars to yield and enters plastic deformation that will not no longer return to the original shape as called strain hardening. Strain is found by the change in length linearly compared to the original length of the specimen as shown in Equation (2-2)

$$e = \frac{\Delta L}{L_0} = \frac{1}{L_0}\int_{L_0}^{L} dL = \frac{L - L_0}{L_0} = \frac{L}{L_0} - 1 \qquad (2\text{-}2)$$

Here, e is the Elastic strain, L_0 and L are the original length and new length of the specimen accordingly.

The density of metal is almost incompressible. In case of very large plastic strains, the density changes by less than 0.1 percent [26]. By considering the volume of a metal is a constant as it is undergoing plastic deformation leading to Equation (2-3)

$$AL = A_0 L_0 \qquad (2\text{-}3)$$

Here, A and A_0 is the new and original cross section area of the specimen accordingly.

The natural strain or true strain ε concept first introduced Ludwik [27] where he used instant changed gage length for the measurement. Mathematically expressed of true strain as follows, where ε is the strain, L is the gage length.

$$\varepsilon = \sum_{1}^{\infty} \frac{L_i - L_{i-1}}{L_{i-1}} = \frac{1}{L_0}\int_{L_0}^{L} dL = \ln\frac{L}{L_0} \quad (2\text{-}4)$$

The equation (2-2) is substitute to the equation (2-4) that given the true strain of the material.

$$\varepsilon = \ln(e + 1) \quad (2\text{-}5)$$

The true stress, σ is define as the applied load to the cross sectional area of the sample. True stress always starts in the plastic region. However, engineering stress rises and then falls after an act the onset of necking. The relation between true stress and the engineering stress are developed by assuming the volume is constant and direction of the strain distribution is same along the length of the specimen shown in equation (2-4).

$$\sigma = \frac{P}{A} = \frac{P}{A_0}\frac{A_0}{A} = \sigma_e(e + 1) \quad (2\text{-}6)$$

The power law equation developed by Ludwik's equation shown in equation (2-5)

$$\sigma = a + b\varepsilon^c \quad (2\text{-}7)$$

The values a, b, and c are arbitrary constants fitted to data from the stress-strain curve. From Ludwik's equation [27] the relation between the elasto- plastic strain hardening and the true stress-strain can be expressed by linear and exponential functions for elastic region and elasto-plastic region accordingly.

$$\sigma = \begin{cases} \varepsilon E & \sigma < \sigma_y \\ \varepsilon_y E + k(\varepsilon - \varepsilon_y)^m & \sigma \geq \sigma_y \end{cases} \quad (2\text{-}8)$$

Here ε_y is the true strain at the yield point where ($\sigma_y = \varepsilon_y E$), k and m are the materials strain hardening coefficient and exponential index respectively. The value for the strain hardening coefficient and exponential index can be exerted by plotting a double logarithm plot to the maximum load from experimental true stress-strain data. These two constant describe completely the shape of the true stress-strain curves. The value of k indicates the level of strength of the material and the magnitude of forces required for testing, while the value of m correlates the slope of the true stress- strength curve [28].

2.3 Indentation Test

In the nano indentation test the indenter impressed into the surface of the test specimen by applied force. Moreover different types of indenters are used for the test which differs on their tip geometry. Almost all the indenter are made from diamond due to its properties of hardness, thermal conductivity and chemical inertness. Generally indenter are two types: Sharp indenter Blunt indenter. Cones and Pyramid are define as Sharp indenter. On the other hand cylindrical flat punch and Spherical indenters are the Blunt indenter.

Berkovich is a three sided pyramidal indenter which have three intersecting polished planes approach congenitally make a sharp point tip. The apex angle of the Berkovich indenter is 65.3^0 which provide the equal area to depth ratio same as the Vickers indenter. Vickers indenter has four sided with polar faces at a semi-angle $\alpha=68^0$ which make $\beta=22^0$ with the specimen surface [29]. The knoop indenter has two different semi-angle with four sided pyramidal. The cylindrical flat punch indenter is more uniform and simply characterized by the tip diameter and requires few parameter for computing the indentation pressure. It has constant contact area during the indentation process and it quickly outstretch to the hemi- spherical elastic plastic condition whereas the contract area varies with time for the other indenters.

2.4 Load Displacement Curve

Load displacement curve is important factor to figure out the mechanical properties in the nano indentation process. Load is applied from zero to maximum in small increments during loading process and plastic deformation happens in the surface of the specimen. During the unloading process load is reverted to zero from the maximum value and the specimen tries to reform its original shape but plastic deformation prevents the full recovery. In the load-depth curve the loading portion has both elastic and plastic retaliation where the unloading segment mention to entirely elastic allowance shown in Fig. 2.2.

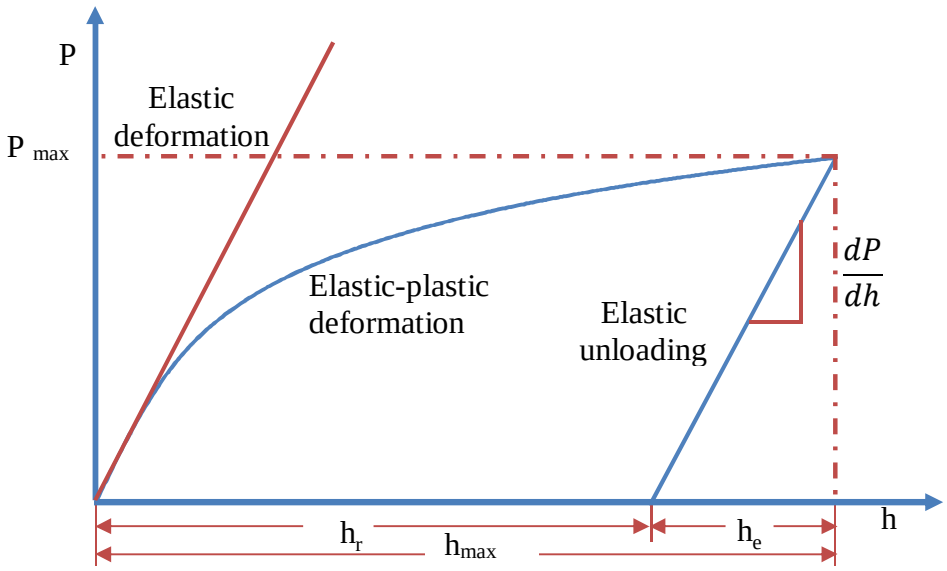

Fig. 2.2: Load Depth curve

Here, the depth of the residual impression h_r, the elastic displacement during unloading h_e, the maximum depth h_{max} from the original specimen surface at maximum load P_{max}.

For cylindrical flat tip indenter during unloading the elastic displacement can be express as follows

$$P = 2aE_r h \tag{2-9}$$

Where a is the contact radius which is equal to the cylindrical flat tip indenter, P is the applied force on the specimen surface. Oliver-Pharr et al [30] [12] proposed a method for calculating the material properties as defined the stiffness S of the material is equal the slop of the initial portion of the unloading curve. The relation between stiffness and the contact area is described in equation (2-7)

$$\frac{dP}{dh} = S = 2\,a\,E_r \tag{2-10}$$

Where E_r is the reduced elastic modulus. From equation (2-7), in terms of contact area can be written as,

$$\frac{dP}{dh} = S = 2\,E_r\sqrt{\frac{A}{\pi}} \tag{2-11}$$

Finally elastic modulus of the specimen E is obtain for the unloading curve using the cylindrical indenter from the following equation,

$$\frac{1}{E_r} = \frac{1-\nu^2}{E} + \frac{1-\nu_i^2}{E_i} \tag{2-12}$$

Here υ_i and E_i are the Poisson's ratio and the Elastic modulus for the indenter and ν and E are the Poisson's ratio and the Elastic modulus for the specimen respectively.

The hardness H is define as the maximum load per unite area can be expressed as following equation,

$$H = \frac{P_{max}}{A} \tag{2-13}$$

Chapter 3 FE Model Formulation and Simulation

3.1 Finite Element modeling

Finite element modeling has been predominantly used in the area of nanoindentation simulation as one of the effective tool to simulate the indentation response at the nanoscale level for more than a decade [31]. Bhattacharya and Nix [32] were the first to use FEM for successfully simulation of the load vs. depth response of sub micrometer indentations on bulk materials. Recently, many researchers have widely adopted FEM since the simulation and analysis of indentation is more complex mathematically and analytically. Huang [33], Pinch [34] [35], Song [36], Poon [37] are used ABAQUAS software for finite element analysis. During recent years ANSYS is most popular software for its spectacular feature and also power full and incredible engineering appliance which can be used to solve the problem with accuracy and reliability of the outputs. Rao and Reddy [38], Chen [39], Strange [40], Gadelrab [41] are used ANSYS software of different version for simulating the finite element analysis. There are some limitations for the finite element model that the total number of elements and computational time is confined.

3.2 Generation of Axisymmetric Model

3.2.1 3-D Geometry Input

Academic FEA software ANSYS version 14.5 ref [42] was used for modeling the indentation test. An axisymmetric model was built assuming that the specimen and indenter are perfect alignment and are symmetrical along the vertical axis. Three different specimen of aluminum 6061T6, AISI1018 and AISI4340 steel are chosen for modeling. A 3-D homogeneous 8 node solid structure element type SOLID 185 was chosen that capable of linear characteristics such as hyperelasticity, elasto-plastic stress strain, large strain stress stiffening and deflection. A 3-D target segment TARGET 170 and 3-D 4 node surface to surface contract element CONTA 173 was employed for indenter and the specimen accordingly. The target element was used to represent various target surfaces for the identified contact elements. Contact takes place when one of the target segment elements are penetrated by the element surface on the specified target surface. The nominal diameter for the cylindrical indenter was 10µm and the height was 5µm whereas the actual diameter for testing was 9.318 µm. The dimension of the specimen was 40µm in diameter and 20µm in height. These dimensions are consider to generate half of the model as indenter and specimen. There is no gap between the indenter and the specimen as perfectly aligned model. The maximum indentation depth was selected 0.2 µm to 0.4 µm. The total number of elements and nodes are 29171 and 31591 respectively. The origin of the Cartesian coordinate system recline at the bottom surface of the indenter in the center. The Geometry of the model is shown in Fig. 3.1 and Fig. 3.2 displays the areas of the half model.

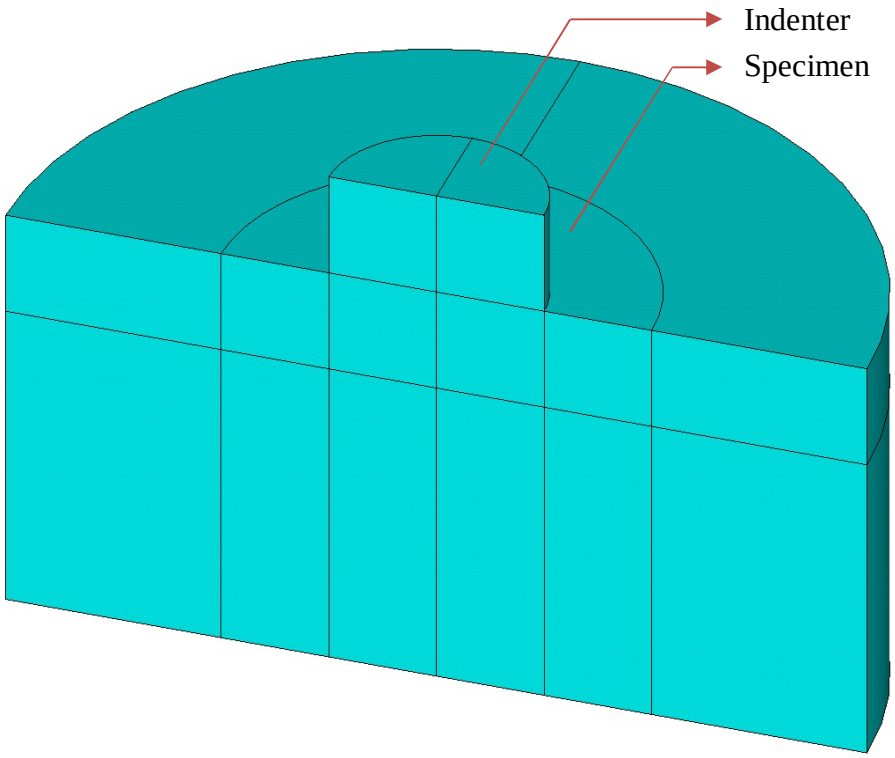

Fig. 3.1: 3-D symmetric model

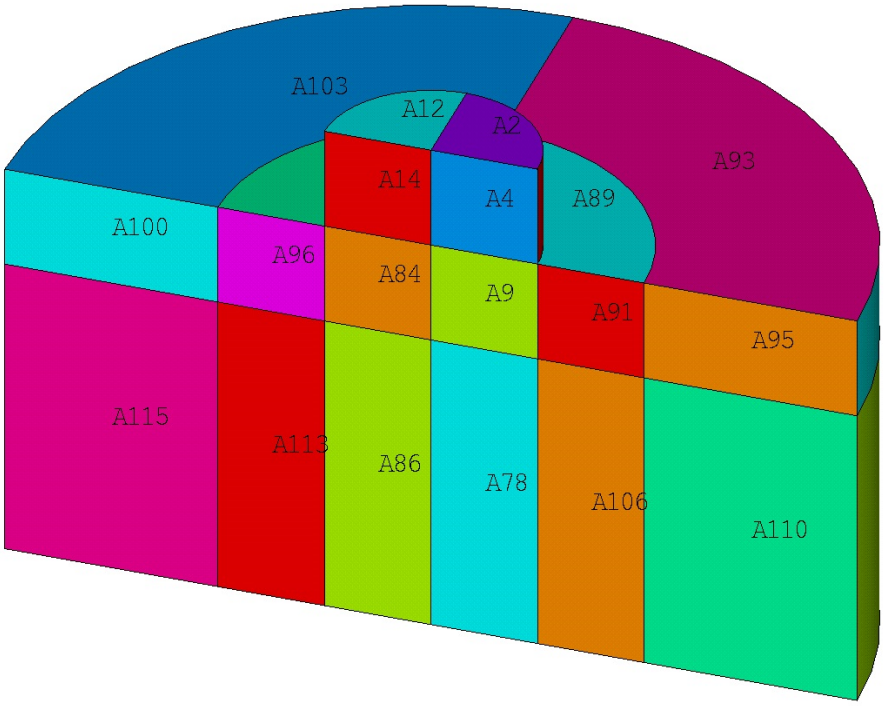

Fig. 3.2: Area for the indenter and specimen

The 3-D comprehensive model is shown in Fig. 3.3. The mechanical properties of the specimen measured by the nanoindentation modeling is sensitive to the thickness of the specimen. A non-linear spring damper element COMBIN39 was used vertically to restrain the effect of thickness connected to each node with the bottom of the specimen. The length of the spring damper was 5 µm and considered that there was no mass of the spring even no bending or torsion.

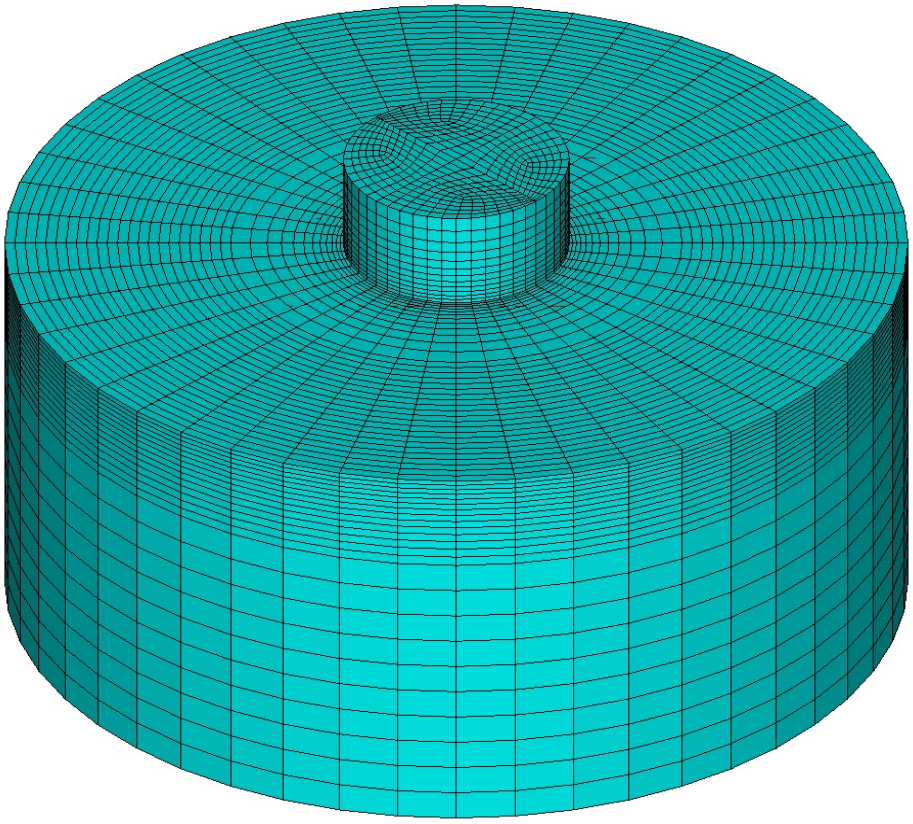

Fig. 3.3: 3-D comprehensive model

3.2.2 Mesh the Model

The mesh density and the refine are very important to improve the accuracy of the model when having a small displacement with a large force. Hence, the region of interest lies directly underneath the indenter was used comparatively denser around the edge of the indenting area as the deformation during the indentation process is primarily concentrated near that region. However, due to the limitation of current version of ANSYS software, a robust amount of elements were not possible to employ in the current 3-D model. By considering the convergence of the load-depth curve and the limitation of the total number of elements and nodes, the element size were determined for the model which shown in Fig. 3.4 and Fig. 3.5. Mapped meshing was chosen for the simulation.

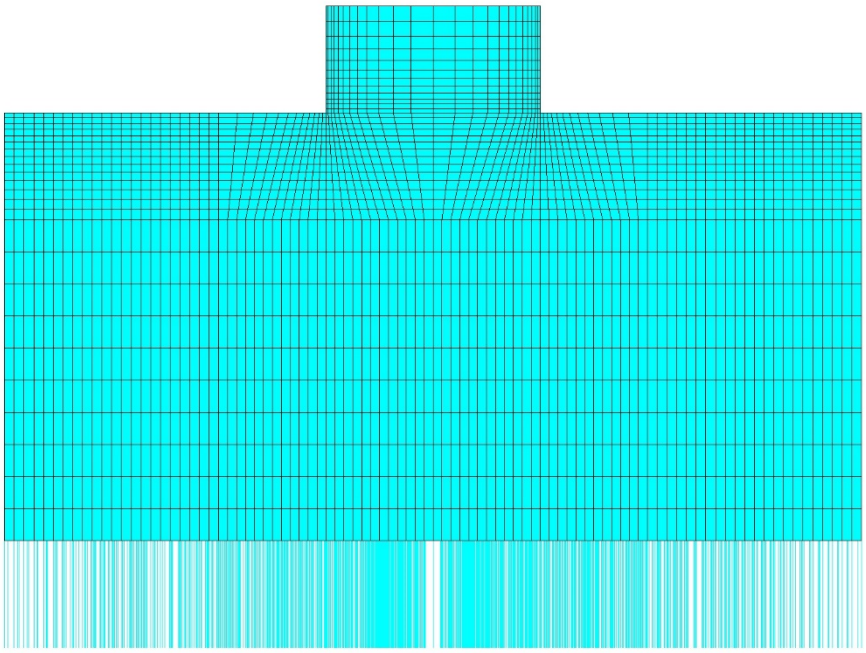

Fig. 3.4: Mesh exemplification for the 3-D symmetric model

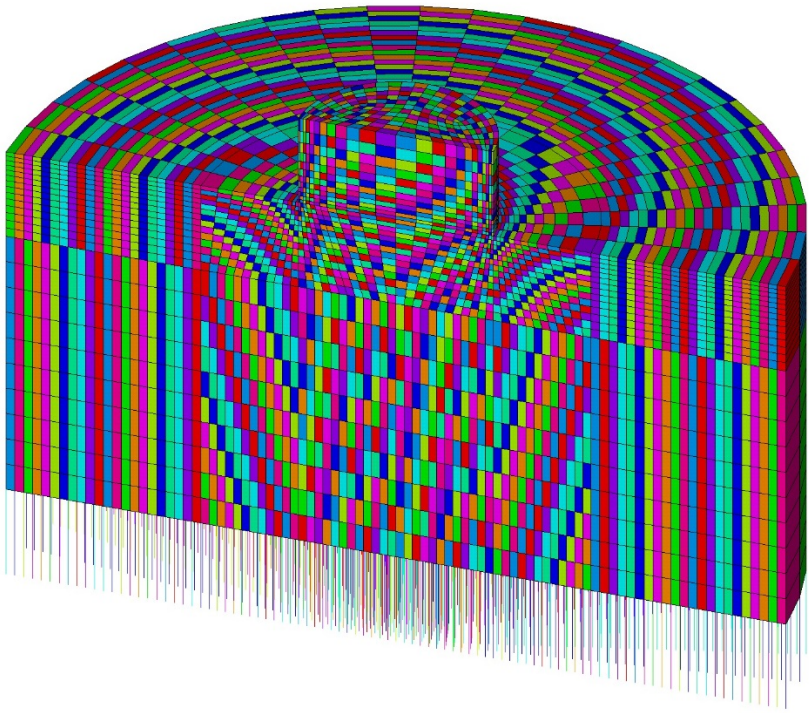

Fig. 3.5: Meshed elements of the model.

3.2.3 Boundary Condition

To get an authentic solution, appropriate boundary condition as well as the loading condition is a crucial factor. The displacement of the boundary condition is set such as all the nodes on the y axis can only have the displacement in the y direction. The indenter upper surface all the nodes have the displacement only y direction and can move only y direction during the loading and unloading step. The other direction x and z direction is set to zero shown in the Fig. 3.6 and Fig. 3.7 boundary constraints for the model. The spring elements are associated vertically to each node at the bottom surface of the specimen where the other end of the spring element is constrained i.e. all the nodes can’t shift any direction as a result this suppress the specimen from sliding when the

sample is indented. The damping coefficient was used 4.5 micro Newton sec per micro meter for this model.

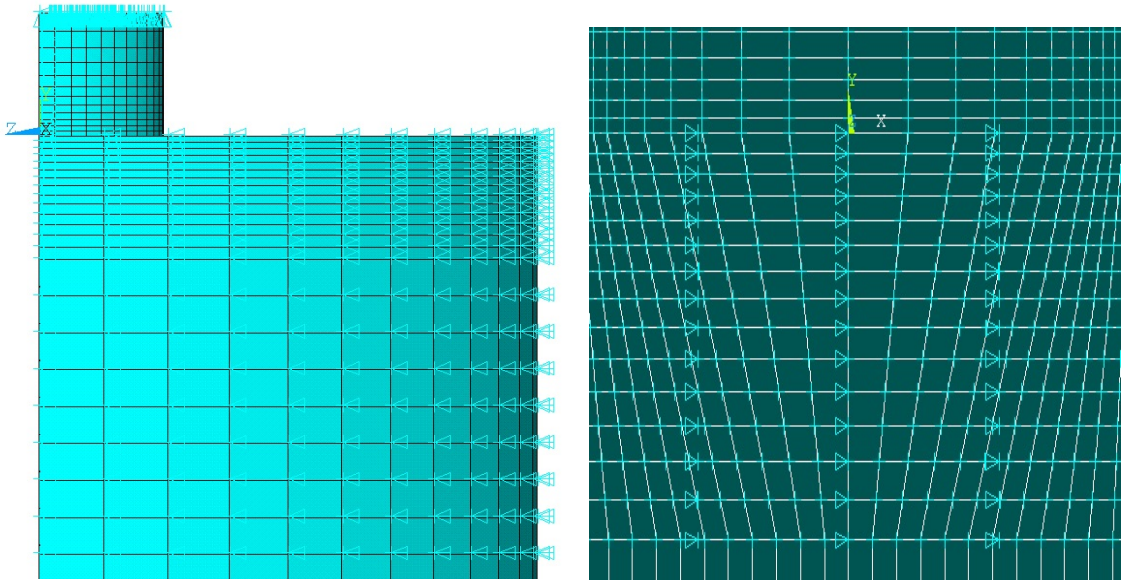

Fig. 3.6: Boundary conditions Z axis and X axis of the model.

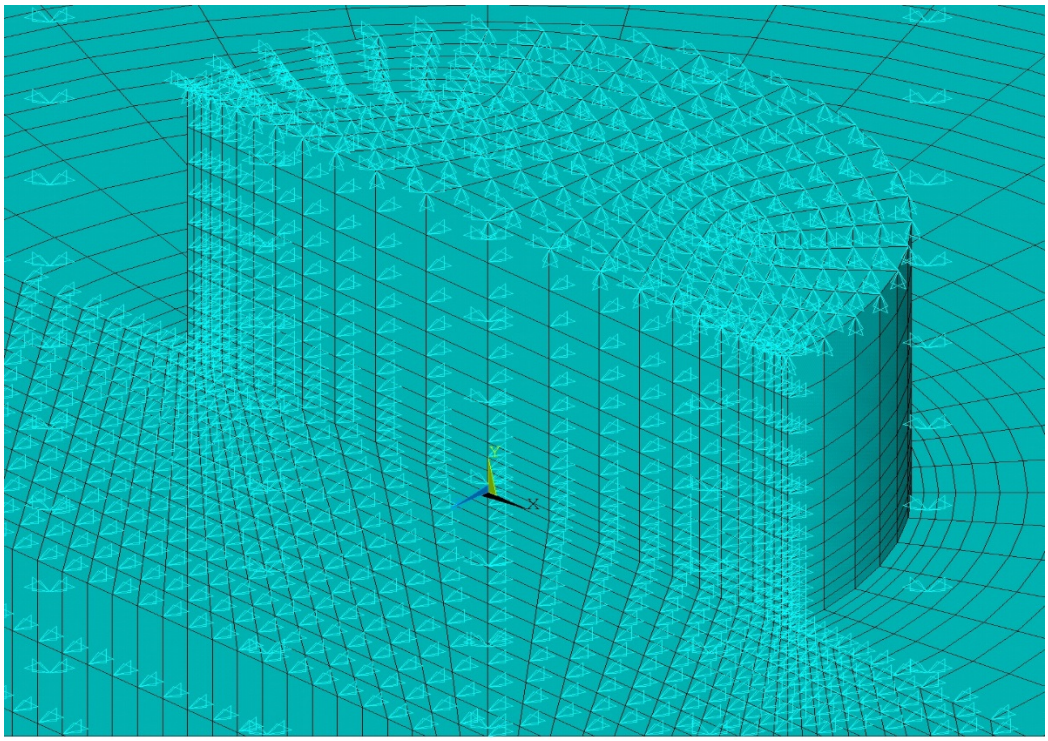

Fig. 3.7: Boundary constraints of the model.

3.2.4 Apply Load

There was two load steps used in the modeling where one is loading and the other one is unloading. During the loading step, indenter displacement is applied towards the y direction on the specimen up to the maximum indentation depth shown in Fig. 3.8 . During the unloading step, the indenter returns to its original position incrementally, the indenter was lifted up to the half of its way back to the original position as the load becomes zero before reaching that depth.

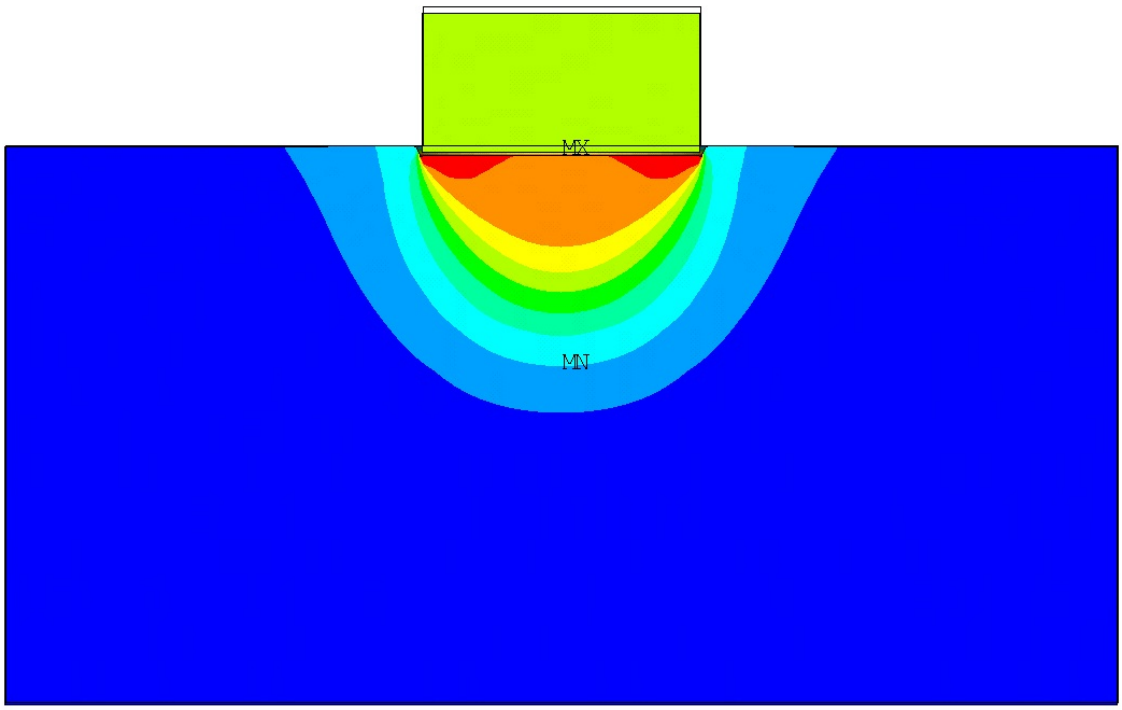

Fig. 3.8: Graphical representation of displacement during loading

Chapter 4 Result and Discussion

4.1 Model Validation

After completing the model the true stress and strain values obtained from the tensile test were imported into ANSYS batch file. The friction coefficient was set for the model was 0.15 based on the research accomplish by Yurkov [43]. There was sliding friction of diamond on steel and aluminum which can be ignored. Hu et al [44] showed that the friction coefficient on indentation testing varied between 0.1 and 0.2 of diamond indenter on AISI1018, AISI4340 and 6061T6 which is less effect on yield strength.

The load displacement data from the tensile tests were converted in to engineering stress-strain data. The average true stress-strain curves of each material are shown in Fig. 4.1 that compare the experimental and the theoretical results.

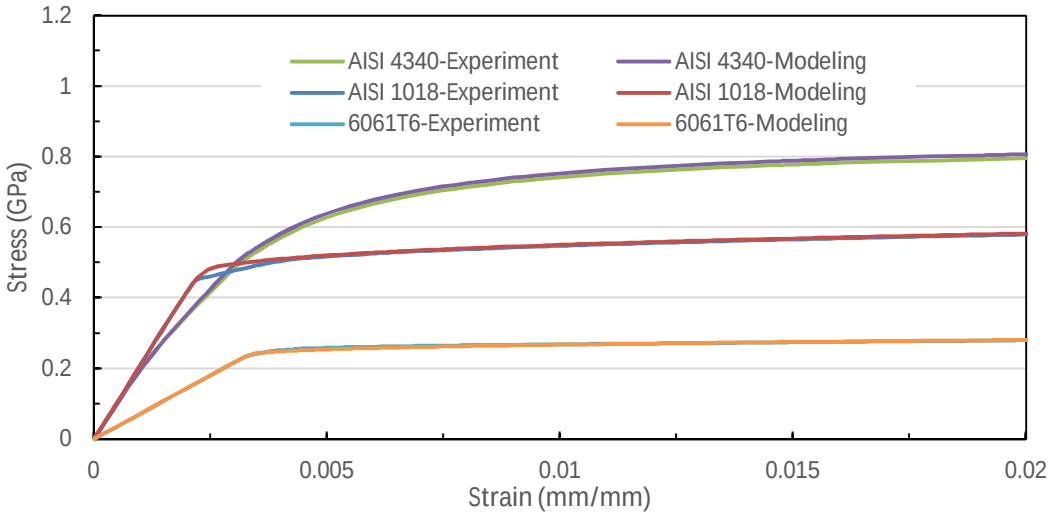

Fig. 4.1: Average true stress-strain curves for materials of AISI 4340, AISI 1018 and 6061T6

To validate the modeling results obtained from FEM simulations, corresponding nanoindentation experimental results [44] were used to compare the indentation profiles. Load-depth response for cylindrical flat tip indentation of AISI 4340, AISI 1018 and Aluminum for modeling and experimental data can be seen from Fig. 4.2. The modeling L-D curve is much harder whereas it appears to be quite stiffer having higher loads compared to the experimental load-depth curve.

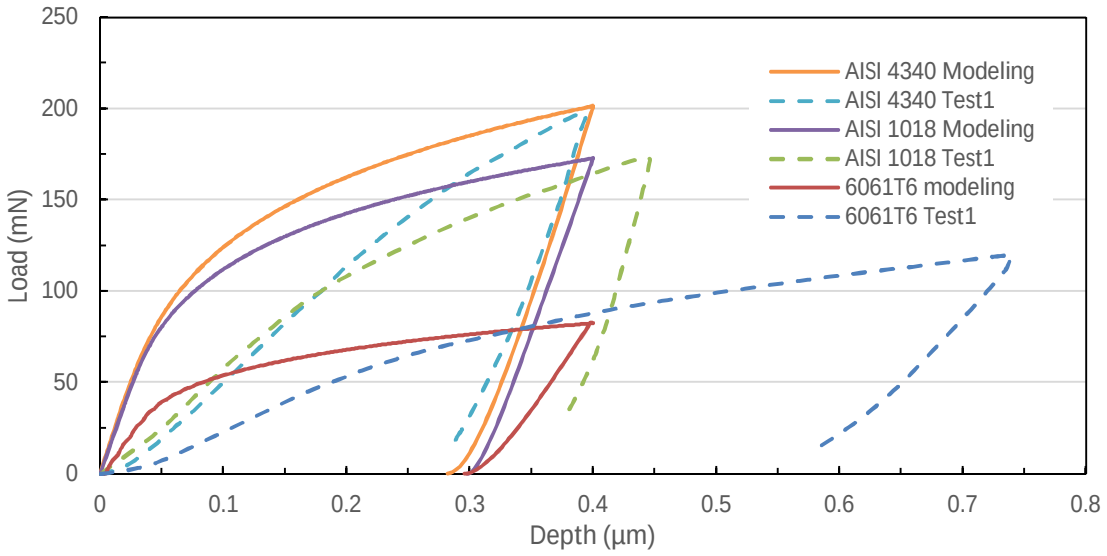

Fig. 4.2: Sample load vs depth curves of the different material corresponding Poisson ratio 0.3

From 3-D modeling result the average elastic modulus and the hardness for AISI1018 are 209.24 GPa and 2.02 GPa and from 2-D modeling result [44] the elastic modulus and the hardness are 208.96 GPa and 2.06 GPa respectively which varies within 0.1339%.

4.2 Model of AISI-1018

4.2.1 Effect of Poisson ratio on maximum indentation depth

Load depth respond for cylindrical flat tip indentation for modeling data can be shown in Fig. 4.3, Fig. 4.4 and Fig. 4.5 based on maximum depth 0.4µm, 0.3µm and 0.2µm accordingly.

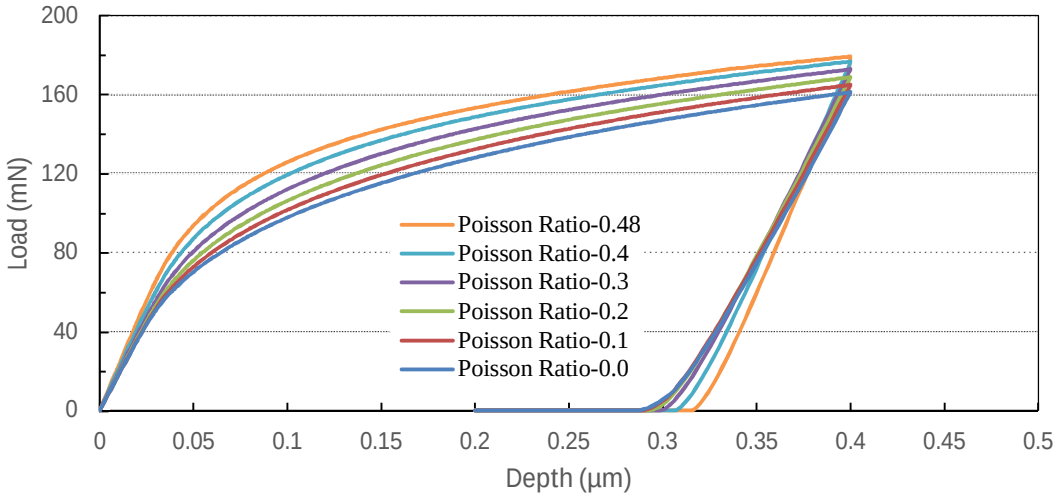

Fig. 4.3: Load displacement curve for h_{max} 0.4 µm

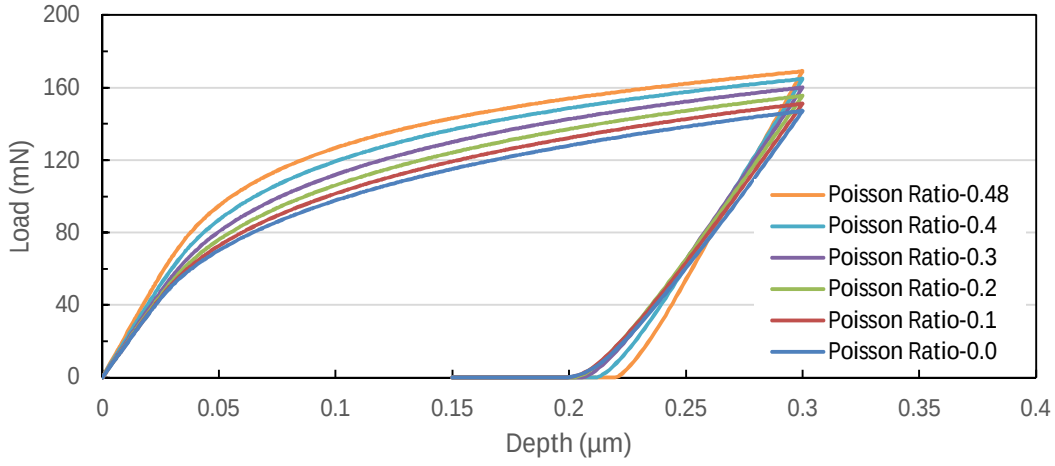

Fig. 4.4: Load displacement curve for h_{max} 0.3 µm

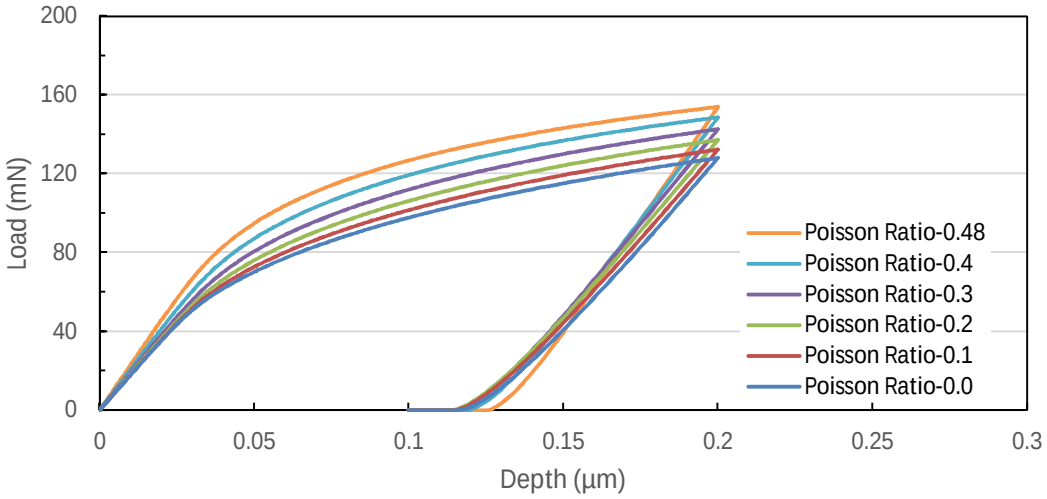

Fig. 4.5: Load displacement curve for h_{max} 0.2 µm

From the modeling results of load depth curves, it is clear that the indentation load increased with the increase of Poisson ratio for the different indentation depth. The modeling L-D curve appears to be quite stiffer having higher load with the increase of Poisson ratio where the maximum indentation depth is same. The indentation depth has very little effect on material properties of the specimen corresponding the same Poisson ratio.

4.2.2 Effect of hardness

The hardness slowly increases, almost linearly, as maximum indentation depth increases. The difference is within ±6.5 when maximum depth ranges from 200 nm to 400 nm which corresponds to the maximum indentation load of 128.05 mN to 179.06 mN as shown in Fig. 4.6.

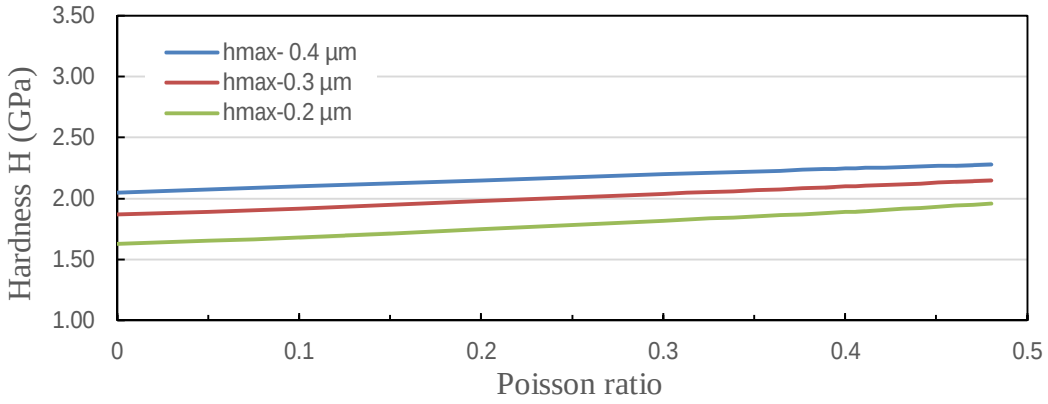

Fig. 4.6: Effect of Poisson ratio on hardness

In the same Poisson ratio the hardness of modeling data is almost constant, while the testing data [45] shows fluctuation due to strain hardening shown in Fig. 4.7.

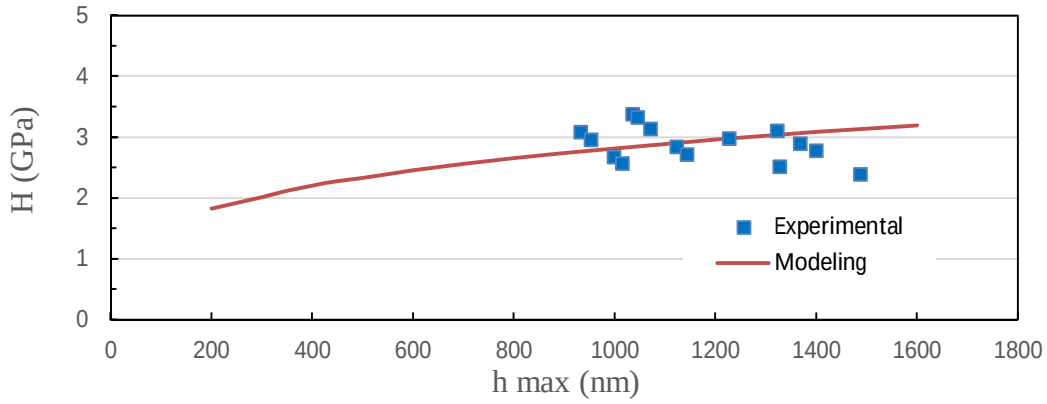

Fig. 4.7: Compare hardness data corresponding Poisson ratio 0.3

4.2.3 Effect of Elastic Modulus

The data shown in Fig. 4.8 indicates that the elastic modulus doesn't vary with different maximum indentation depth. The elastic modulus slowly increases with the increase of Poisson ratio. It was found that the value for elastic modulus ranges from 204 to 220 GPa with different Poisson ratio.

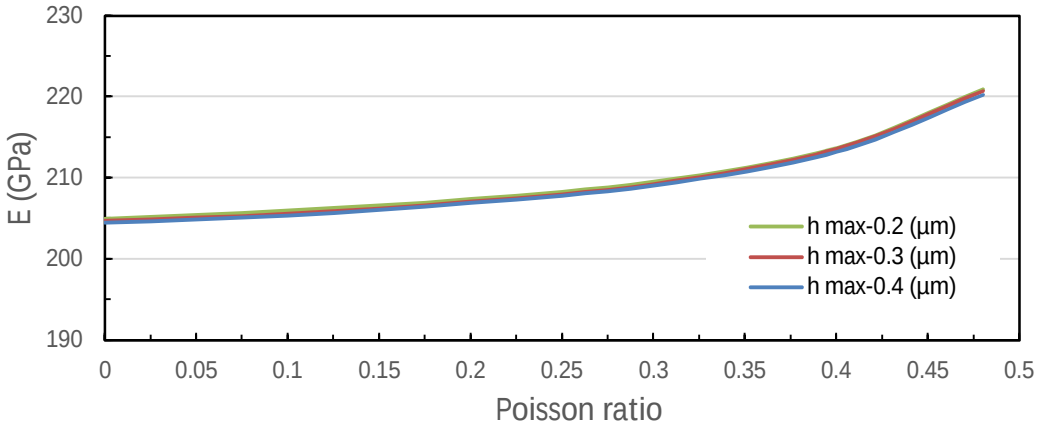

Fig. 4.8: Effect of Poisson ratio on Elastic Modulus

From modeling it can be seen that elastic modulus varies within 0.14% with respect to depth in the same Poisson ratio. The average experimental modulus of elastic was 211.58 GPa [45] that varies within 1.09% from the modeling shown in Fig. 4.9.

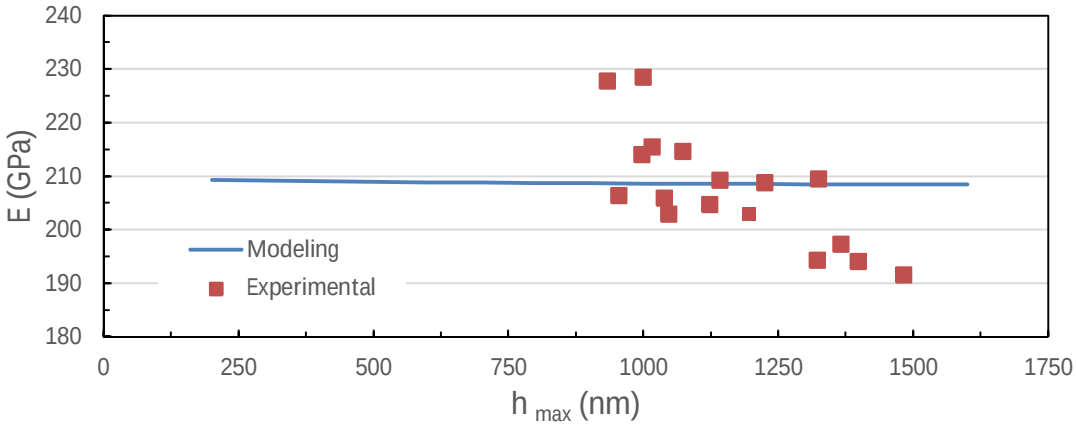

Fig. 4.9: Compare Elastic modulus corresponding Poisson ratio 0.3

4.2.4 Effect of Maximum load

The maximum indentation load obtained by FE simulation 179.065 mN when the Poisson ratio is 0.48 in the h_{max} 0.4 µm. From the modeling results shown in Fig. 4.10, it is clear that the indentation load increased with the increase of Poisson ratio for the different indentation depth. The average experimental max load varies within 10% from the modeling data shown in Fig. 4.11.

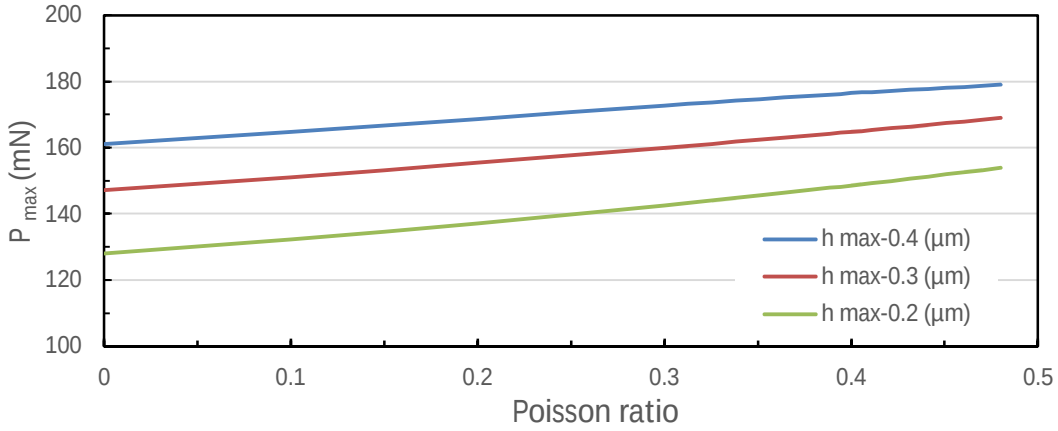

Fig. 4.10: Effect of Poisson ratio on maximum load

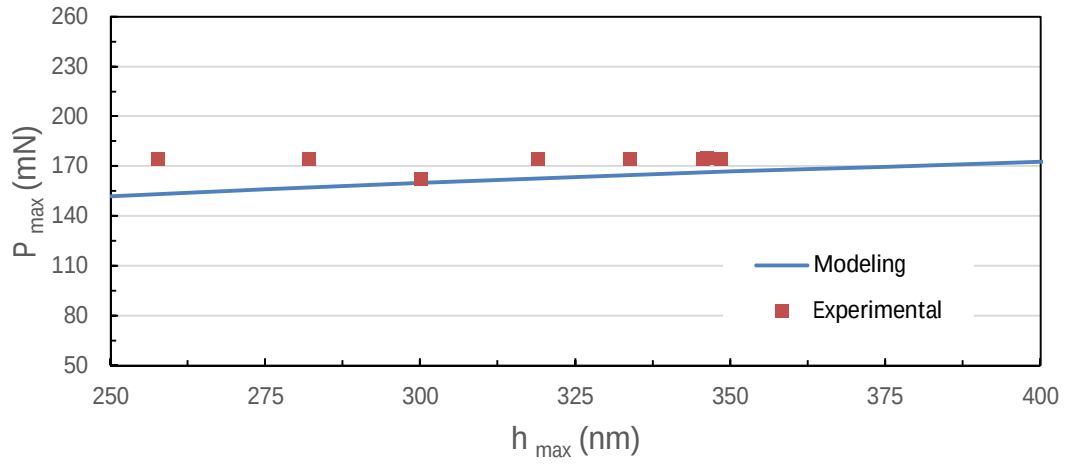

Fig. 4.11: Compare maximum load data corresponding Poisson ratio 0.3

4.2.5 Effect of Maximum Pile Up

From the Fig. 4.12 it can be seen that the deeper the maximum indentation, the higher the maximum pile up. It was found that the value for maximum pile up ranges from 6 to 91 nm with different Poisson ratio which is very sensitive. The average experimental maximum pile up measured by the laser microscope varies within 10% from the modeling data shown in Fig. 4.13 in the same Poisson ratio.

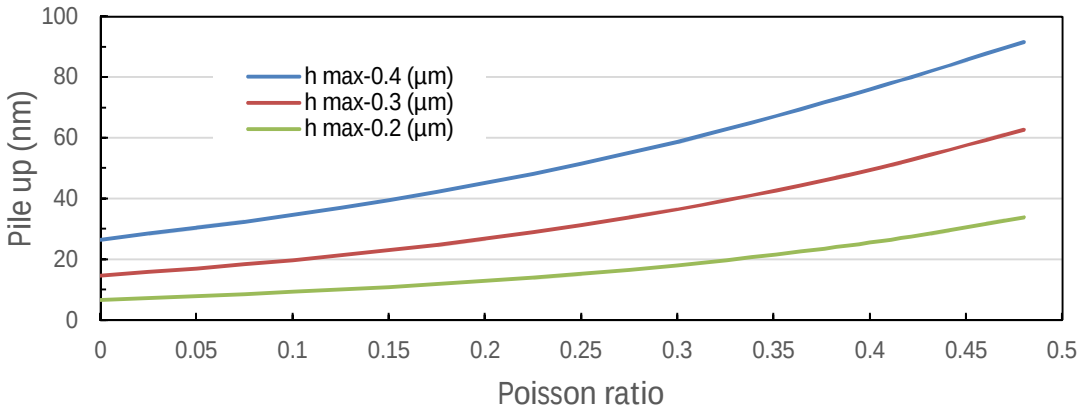

Fig. 4.12: Effect of Poisson ratio on maximum Pile up

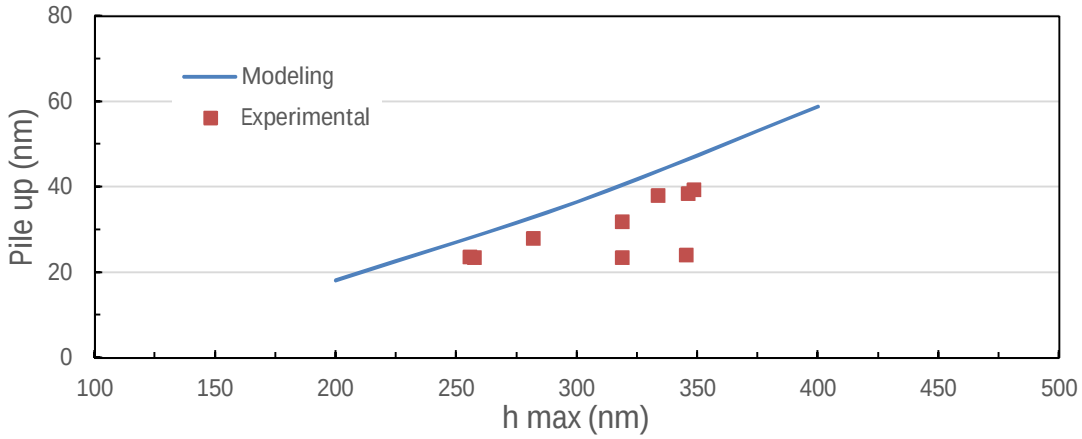

Fig. 4.13: Compare maximum Pile up corresponding Poisson ratio 0.3

Fig. 4.14, Fig. 4.15 and Fig. 4.16 shows the pile up curve with different depth corresponding to the Poisson ratio from 0 to 0.48 of Steel 1018.

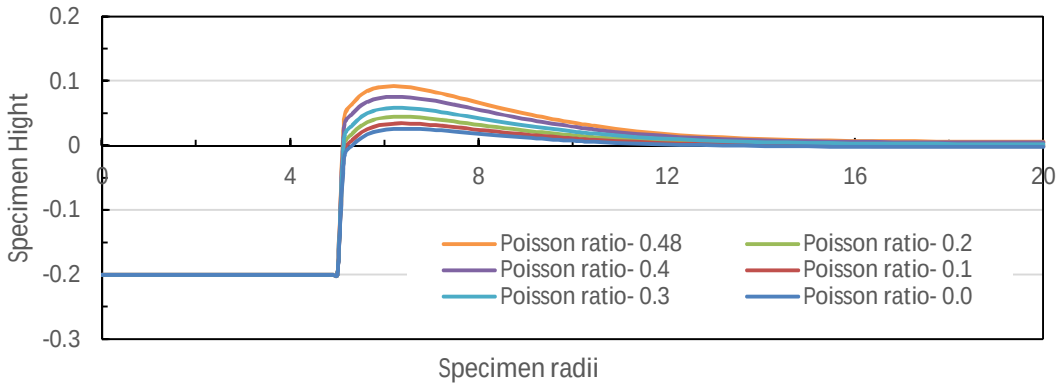

Fig. 4.14: Pile up curve corresponding to Poisson ratio with h_{max} 0.4 µm

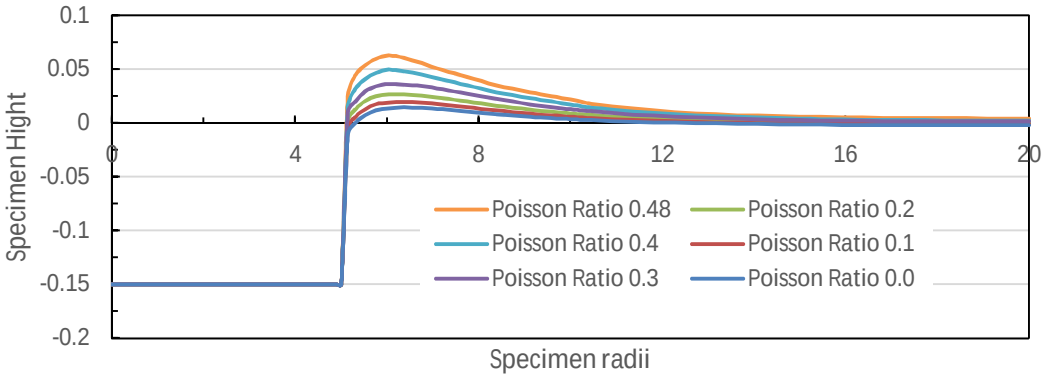

Fig. 4.15: Pile up curve corresponding to Poisson ratio with h_{max} 0.3 µm

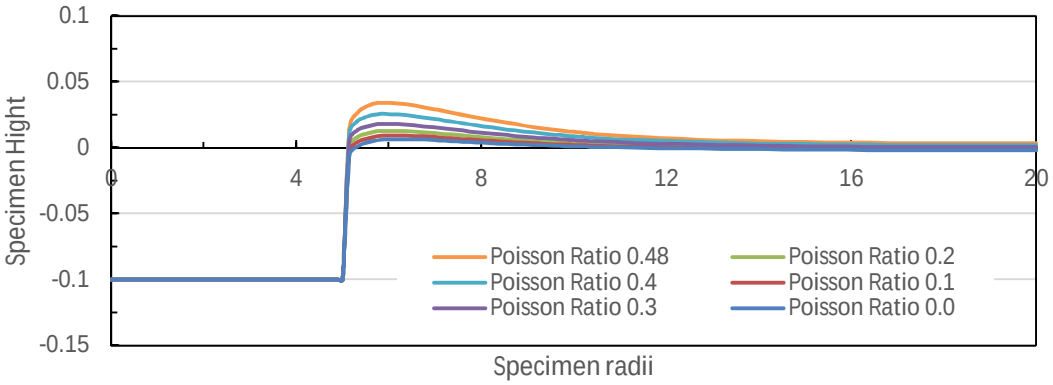

Fig. 4.16: Pile up curve corresponding to Poisson ratio with hmax 0.2 µm

4.3 Model of AISI-4340

4.3.1 Effect of Maximum Indentation Depth

Load depth respond for cylindrical flat tip indentation for modeling data can be shown in Fig. 4.17, Fig. 4.18 and Fig. 4.19 based on maximum depth 0.4µm, 0.3µm and 0.2µm accordingly.

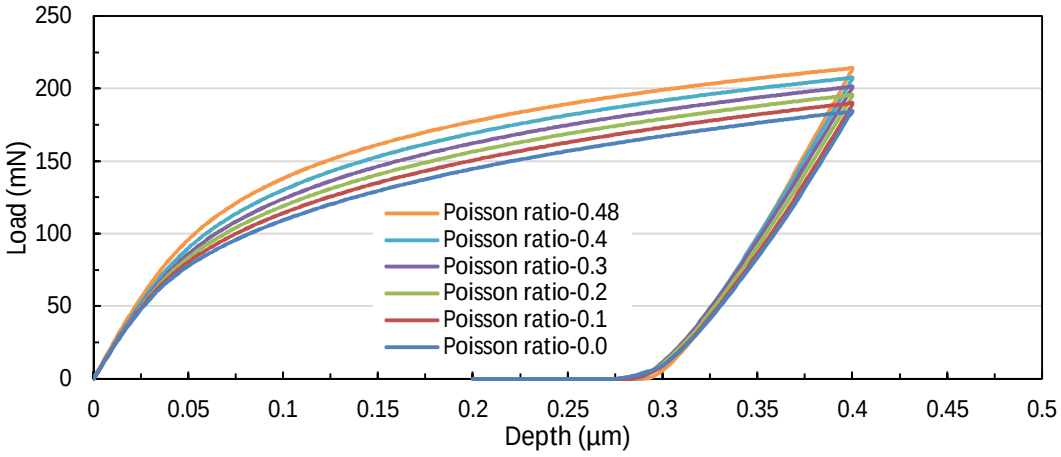

Fig. 4.17: Load displacement curve for h_{max} 0.4 µm

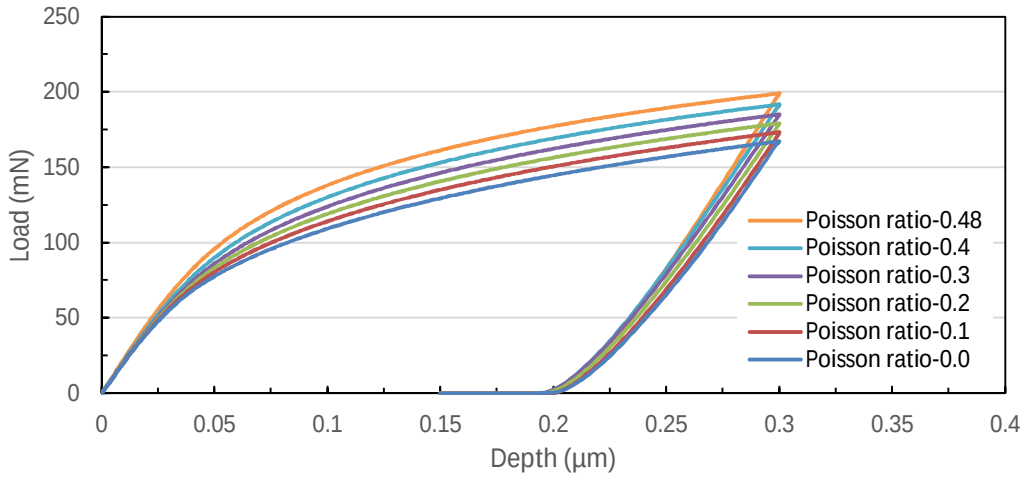

Fig. 4.18: Load displacement curve for h_{max} 0.3 µm

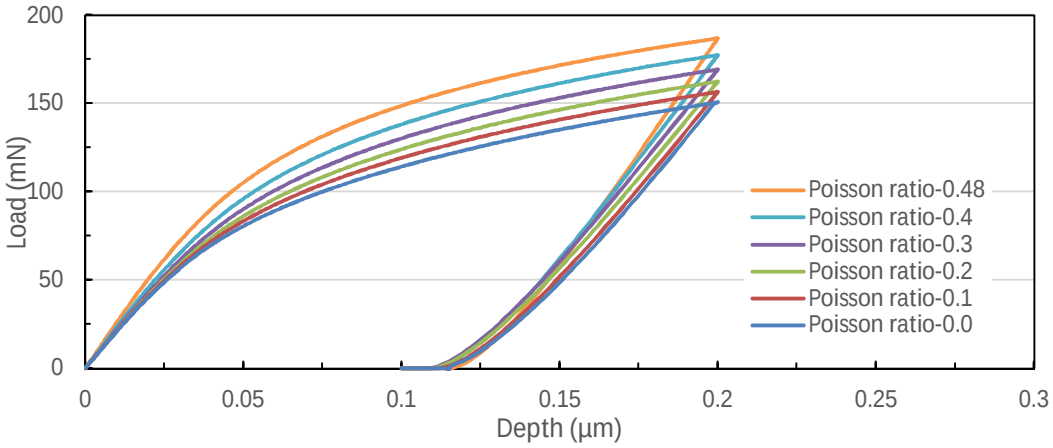

Fig. 4.19: Load displacement curve for h_{max} 0.2 µm

From the modeling results of load depth curves for steel 4340, it is clear that the indentation load increased with the increase of Poisson ratio for the different indentation depth. The modeling L-D curve appears to be quite stiffer having higher load with the increase of Poisson ratio where the maximum indentation depth is same. The indentation depth has very little effect on material properties of the specimen corresponding the same Poisson ratio. The L-D curve of steel AISI 4340 appeared the same shape as steel AISI 1018

4.3.2 Effect of hardness

The hardness slowly increases, almost linearly, as maximum indentation depth increases. The difference is within ±8 when maximum depth from 200 nm to 400 nm which corresponds to the maximum indentation load of 150 mN to 214 mN as shown in Fig. 4.20. From the modeling data in the same Poisson ratio is linear, while the testing data [44] shows fluctuation due to strain hardening shown in Fig. 4.21. The average hardness of steel 4340 is 2.36 GPa corresponding the Poisson ratio 0.3.

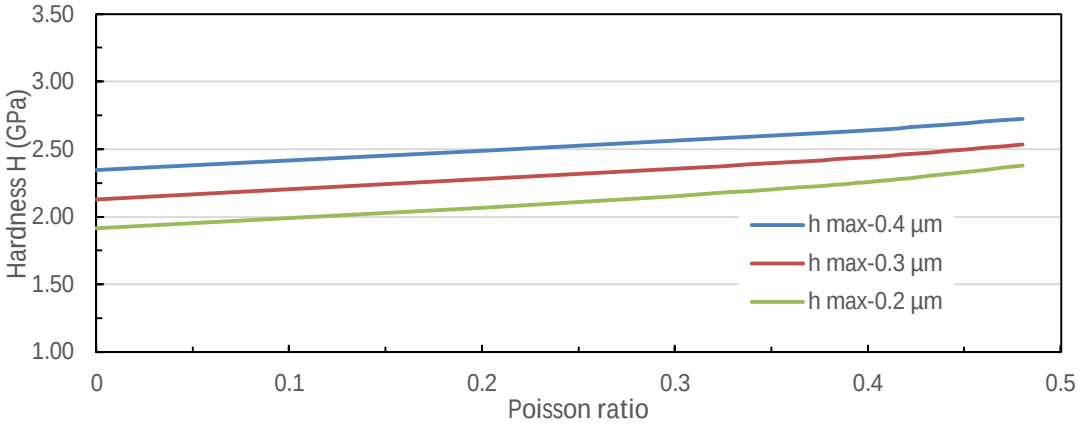

Fig. 4.20: Effect of Poisson ratio on hardness

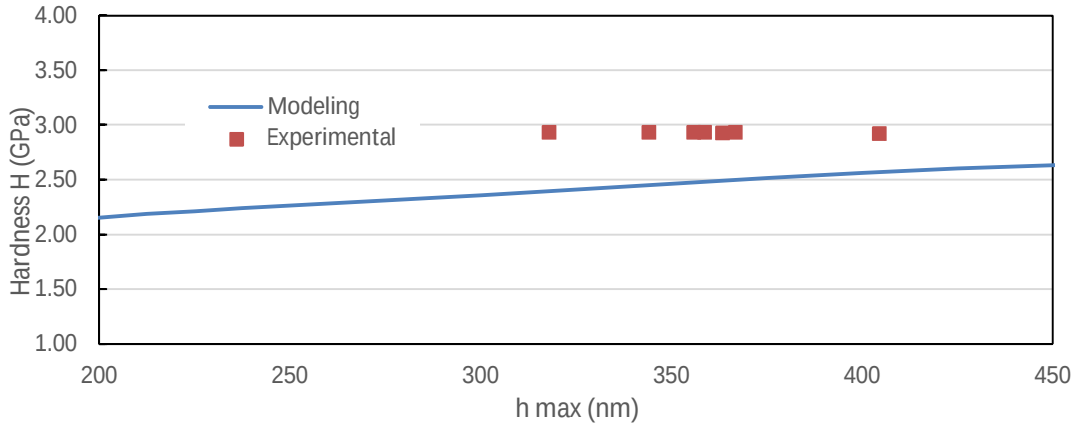

Fig. 4.21: Compare hardness data corresponding Poisson ratio 0.3

4.3.3 Effect of Elastic Modulus

The Fig. 4.22 indicates that the elastic modulus doesn't vary with different maximum indentation depth. The elastic modulus slowly increases with the increase of Poisson ratio, but decrease with the increase of maximum depth. It was found that the elastic modulus ranges from 175 to 200 GPa with different Poisson ratio. From modeling it can be seen that elastic modulus varies within 0.64% with respect to depth in the same Poisson ratio. The average experimental [44] modulus of elastic was 187.84 GPa that varies within 1.72 % from the modeling shown in Fig. 4.23.

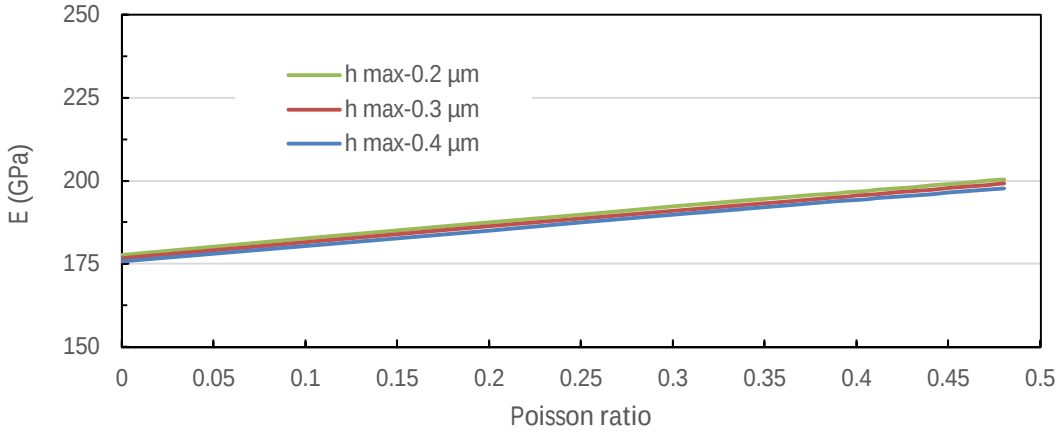

Fig. 4.22: Effect of Poisson ratio on Elastic Modulus

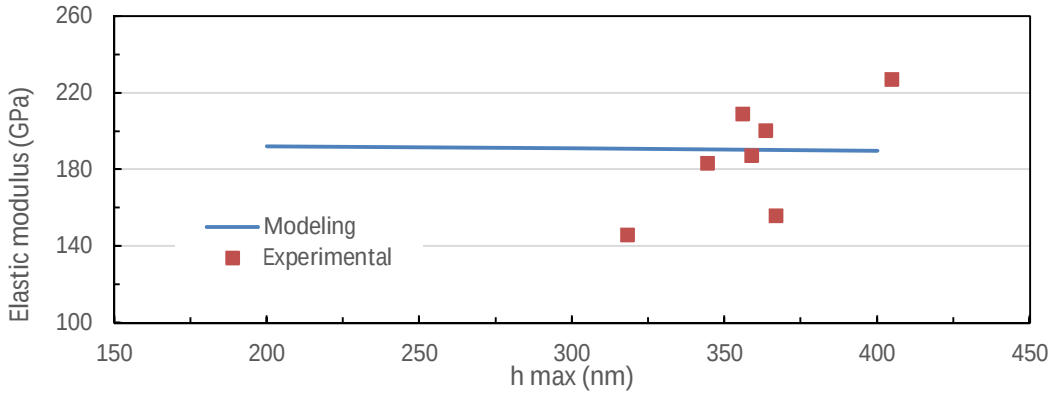

Fig. 4.23: Compare Elastic modulus corresponding Poisson ratio 0.3

4.3.4 Effect of Maximum load

The maximum indentation load obtained by FE simulation 214.16 mN when the Poisson ratio is 0.48 in the hmax 0.4 µm. From the modeling results shown in Fig. 4.24, it is clear that the indentation load increased with the increase of Poisson ratio for the different indentation depth. The average experimental [44] max load varies within 7.61 % from the modeling data shown in Fig. 4.25.

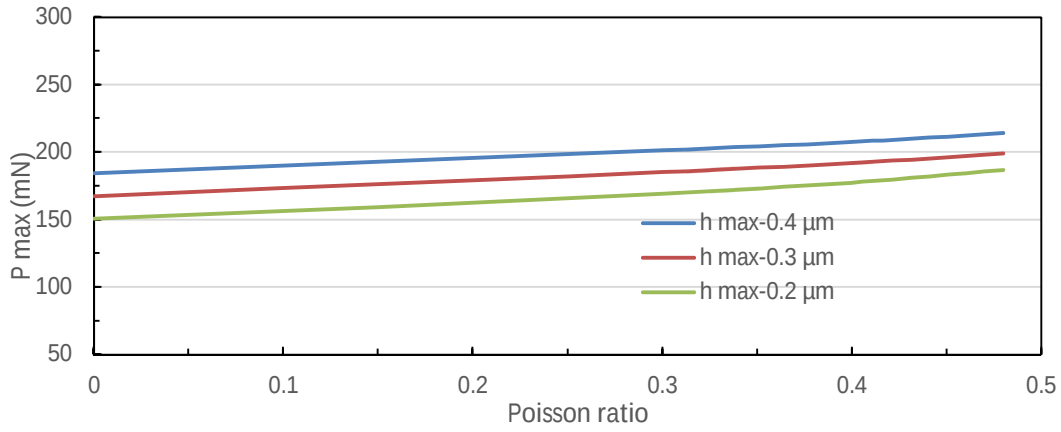

Fig. 4.24: Effect of Poisson ratio on maximum load

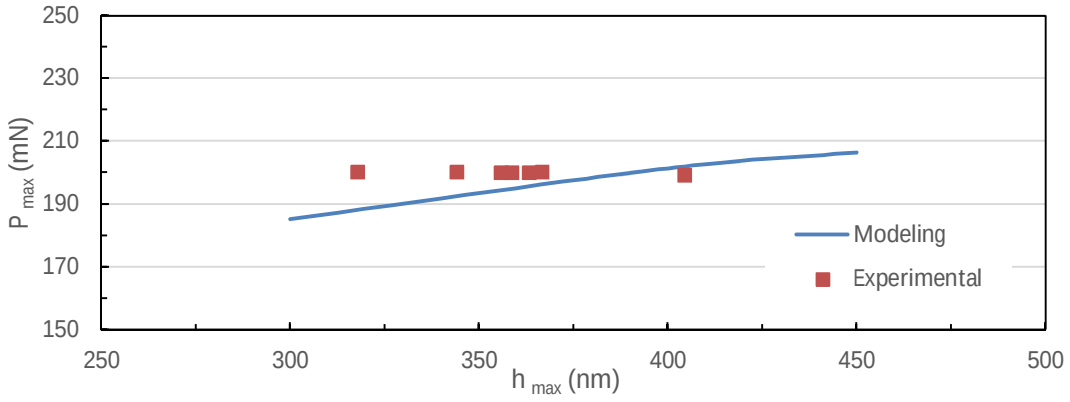

Fig. 4.25: Compare max load data corresponding Poisson ratio 0.3

4.3.5 Effect of Maximum Pile Up

From the modeling data in Fig. 4.26 it can be seen that the deeper the maximum indentation, the higher the maximum pile up. It was found that the value for maximum pile up ranges from 2.72 to 65.03 nm with different Poisson ratio which is very tactful. The average experimental maximum pile up measured by the laser microscope varies within 10% from the modeling data shown in Fig. 4.27 in the same Poisson ratio.

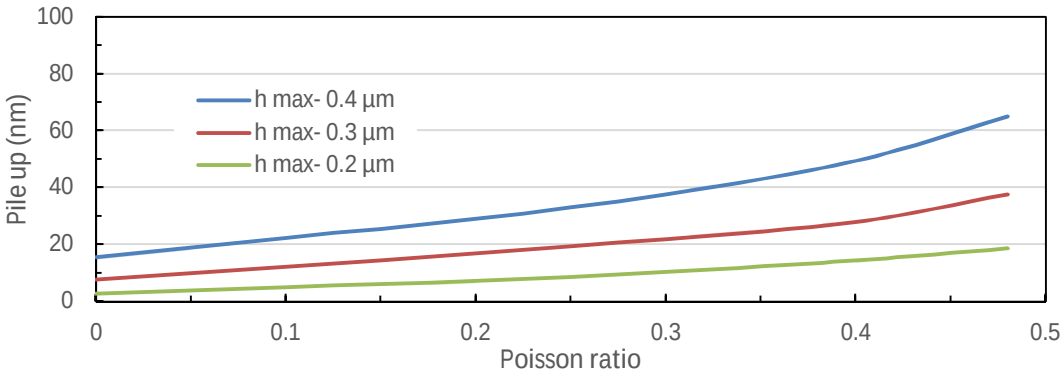

Fig. 4.26: Effect of Poisson ratio on maximum Pile up

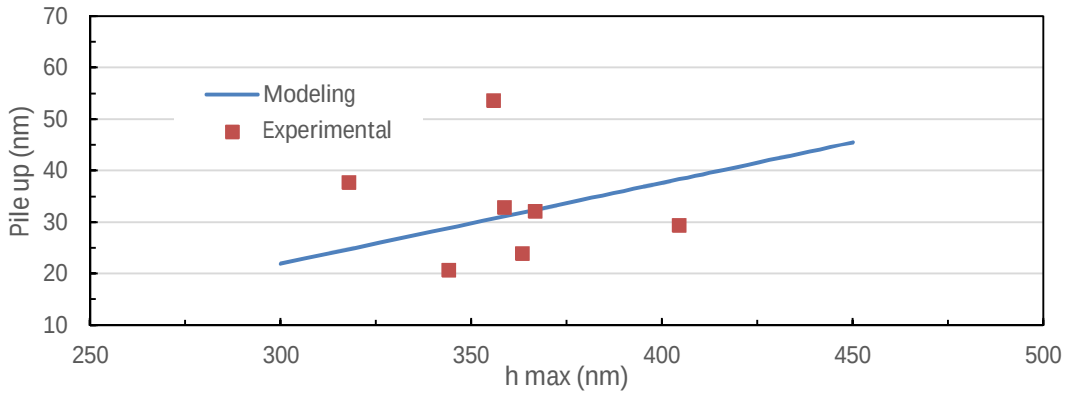

Fig. 4.27: Compare maximum Pile up corresponding Poisson ratio 0.3

The pile up curve with different depth corresponding to the Poisson ratio from 0 to 0.48 of Steel 4340 along the x-y plane to the specimen shown in Fig. 4.28, Fig. 4.29 and Fig. 4.30.

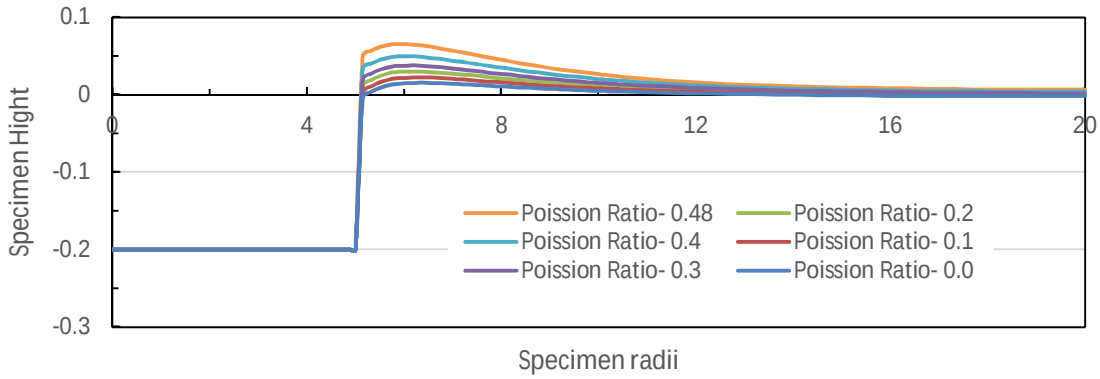

Fig. 4.28: Pile up curve corresponding to Poisson ratio with h_{max} 0.4 µm

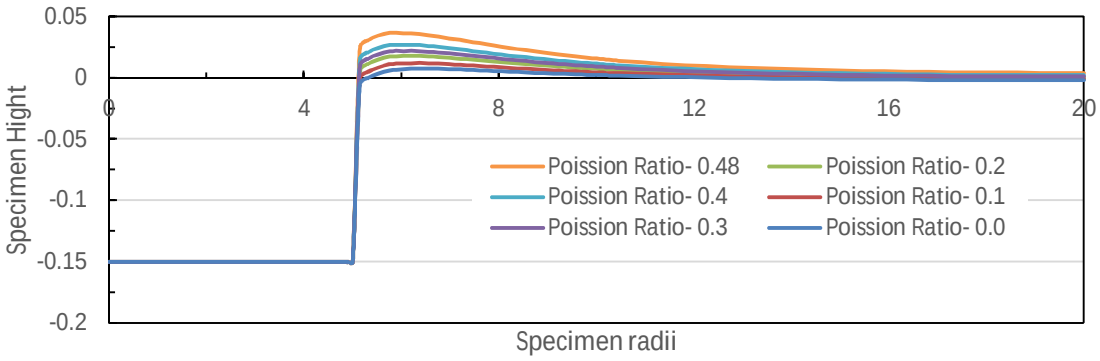

Fig. 4.29: Pile up curve corresponding to Poisson ratio with h_{max} 0.3 µm

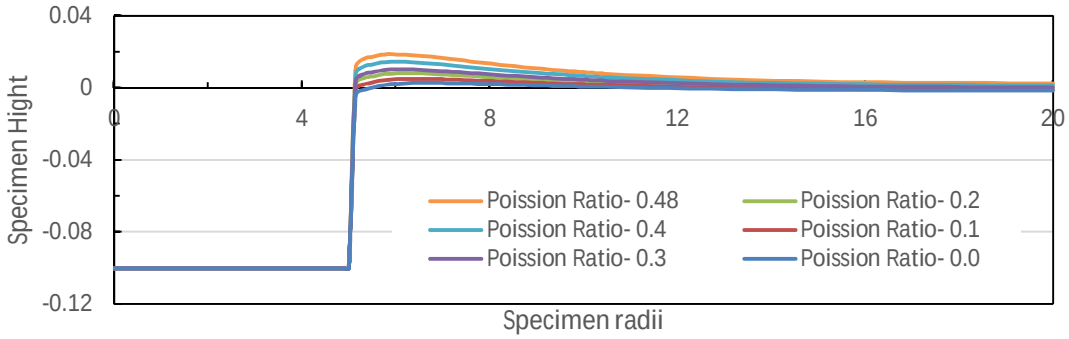

Fig. 4.30: Pile up curve corresponding to Poisson ratio with h_{max} 0.2 µm

4.4 Model of Aluminum 6061-T6

For modeling the dimension of the specimen and indenter are same. However, the mechanical properties of the specimen and the stress strain testing data from testing were imported into ANSYS batch file.

4.4.1 Effect of Maximum Indentation Depth

Load depth respond for cylindrical flat tip indentation for modeling data can be shown in Fig. 4.31, Fig. 4.32 and Fig. 4.33 based on maximum depth 0.4µm, 0.3µm and 0.2µm accordingly.

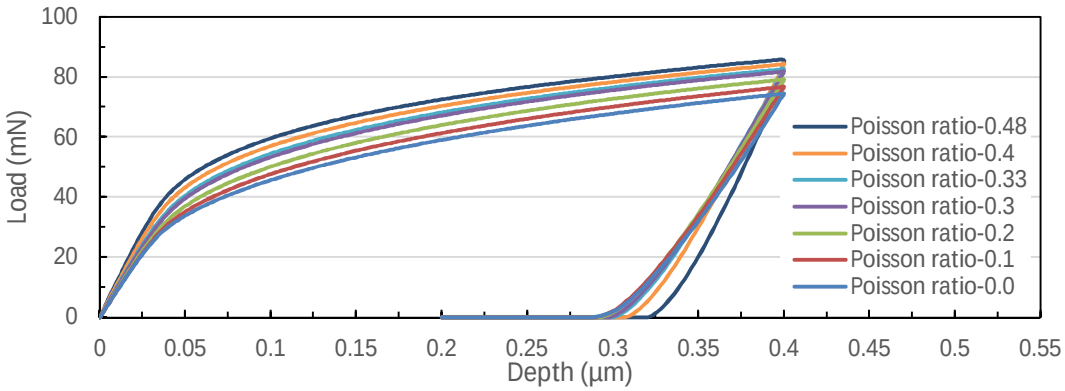

Fig. 4.31: Load displacement curve for h_{max} 0.4 µm

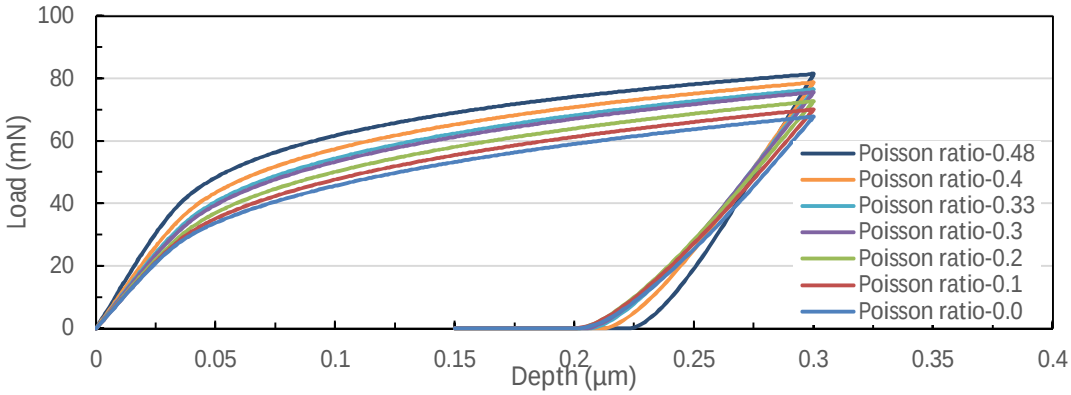

Fig. 4.32: Load displacement curve for h_{max} 0.3 µm

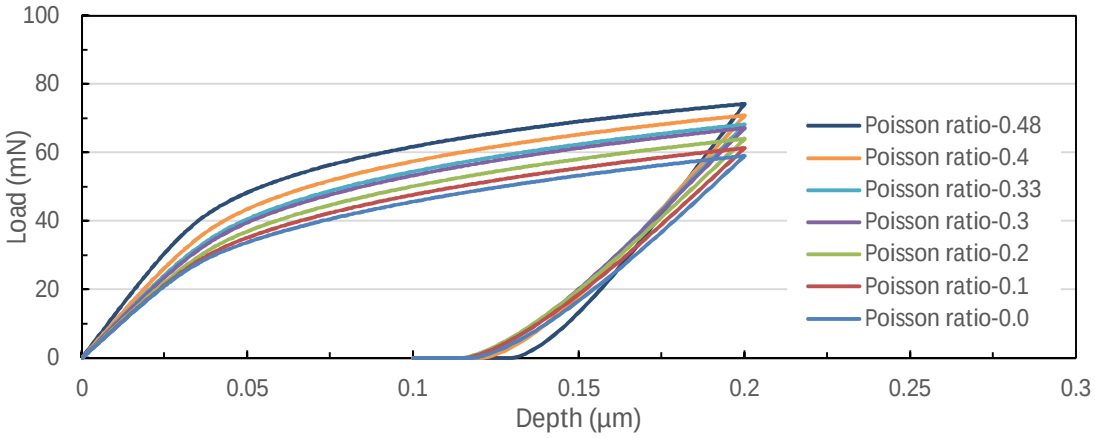

Fig. 4.33: Load displacement curve for h_{max} 0.2 µm

From the modeling results of load depth curves for Aluminum 6061-T6, it is clear that the indentation load increased with the increase of Poisson ratio for the different indentation depth. The modeling L-D curve appears to be quite stiffer having higher load with the increase of Poisson ratio where the maximum indentation depth is same. The indentation depth has very little effect on material properties of the specimen corresponding the same Poisson ratio.

4.4.2 Effect of hardness

The hardness slowly increases with the increase of maximum indentation depth. The difference is within ±8 when maximum depth from 200 nm to 400 nm which corresponds to the maximum indentation load of 68 mN to 83 mN as shown in Fig. 4.34. It can be seen from the testing [44] that the hardness values are higher than the modeling results shown in Fig. 4.35. The average hardness of Aluminum6061T6 is 0.96 GPa corresponding the Poisson ratio 0.33.

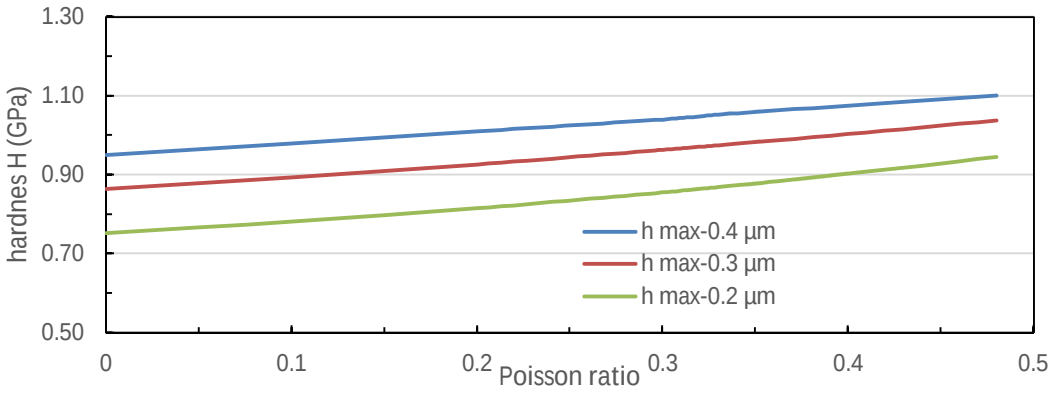

Fig. 4.34: Effect of Poisson ratio on hardness

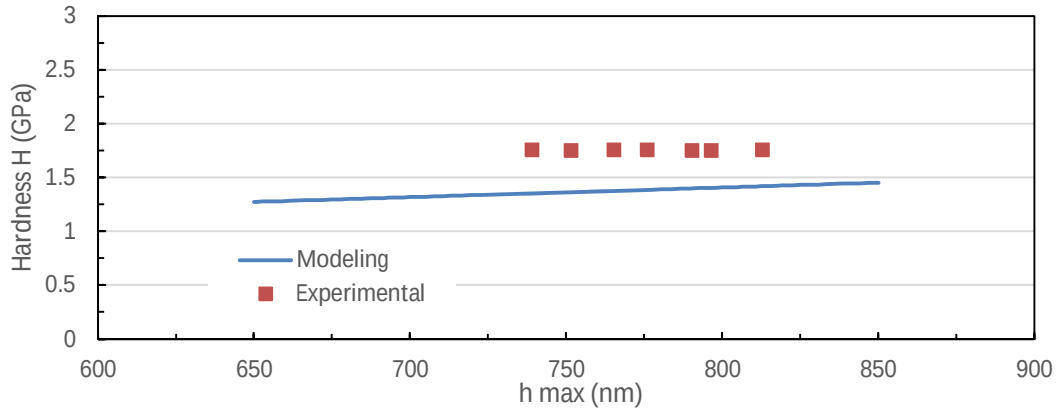

Fig. 4.35: Compare hardness data corresponding Poisson ratio 0.33

4.4.3 Effect of Elastic Modulus

The elastic modulus doesn't vary with different maximum indentation depth indicates in Fig. 4.36. The elastic modulus linearly increases with the increase of Poisson ratio. It was found that the elastic modulus ranges from 63 to 81 GPa with different Poisson ratio. From modeling it can be seen that elastic modulus varies within 0.66% with respect to depth in the same Poisson ratio. The average experimental [44] modulus of elastic was 70.64 GPa that varies within 2.90% from the modeling shown in Fig. 4.37.

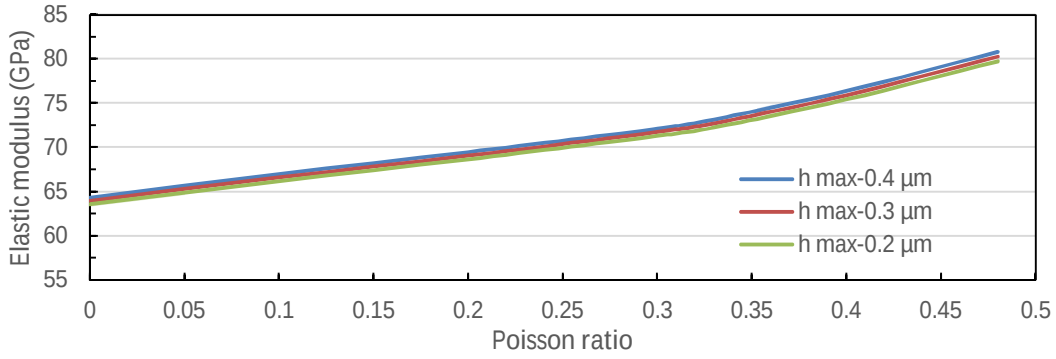

Fig. 4.36: Effect of Poisson ratio on Elastic Modulus

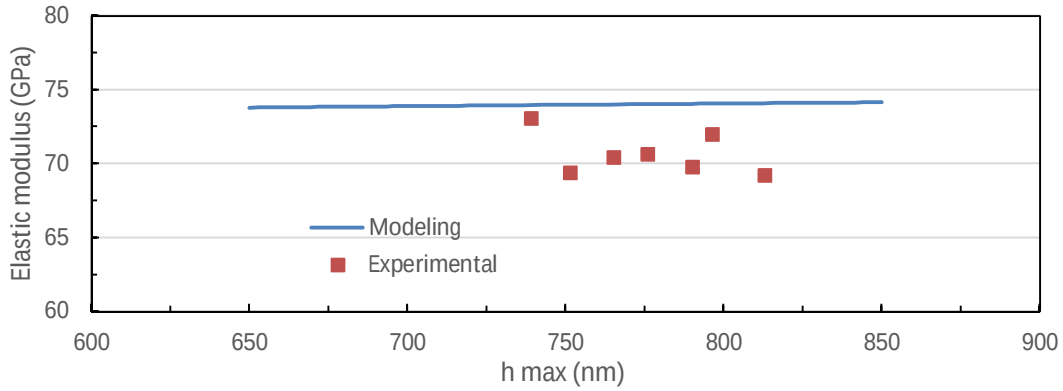

Fig. 4.37: Compare Elastic modulus corresponding Poisson ratio 0.33

4.4.4 Effect of Maximum load

The maximum indentation load obtained by FE simulation 86.39 mN when the Poisson ratio is 0.48 in the h_{max} 0.4 µm. From the modeling results it is clear that the indentation load increased with the increase of Poisson ratio for the different indentation depth shown in Fig. 4.38. The average experimental [44] max load varies within 8.86% from the modeling data shown in Fig. 4.39.

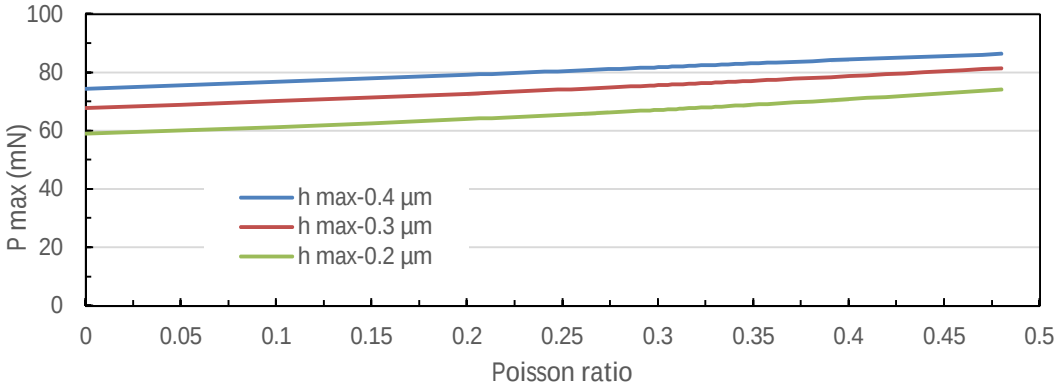

Fig. 4.38: Effect of Poisson ratio on max load

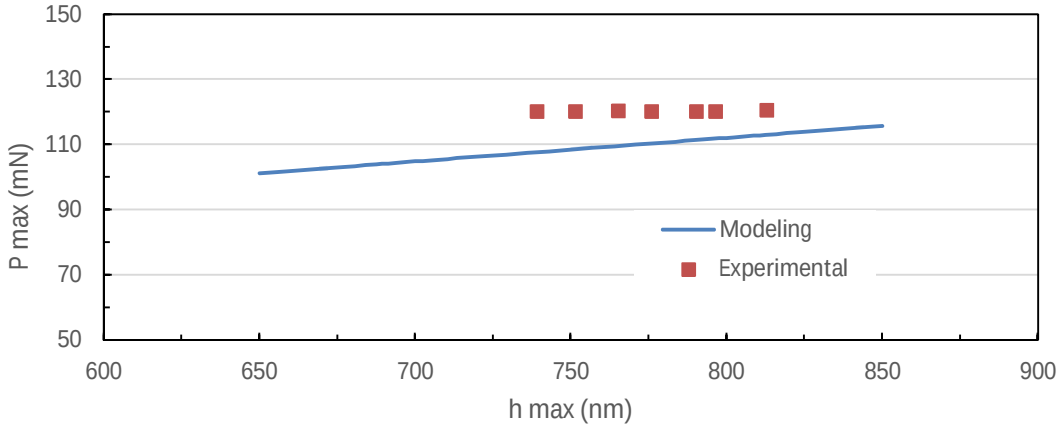

Fig. 4.39: Compare max load corresponding Poisson ratio 0.33

4.4.5 Effect of Maximum Pile Up

From the modeling data of Aluminum 6061 it can be seen that the deeper the maximum indentation, the higher the maximum pile up. It was found that the value for maximum pile up ranges from 7.57 to 93.71 nm with different Poisson ratio which is very tactful shown in Fig. 4.40. The average experimental maximum pile up measured by the laser microscope varies within 16% from the modeling data shown in Fig. 4.41 in the 0.33 Poisson ratio.

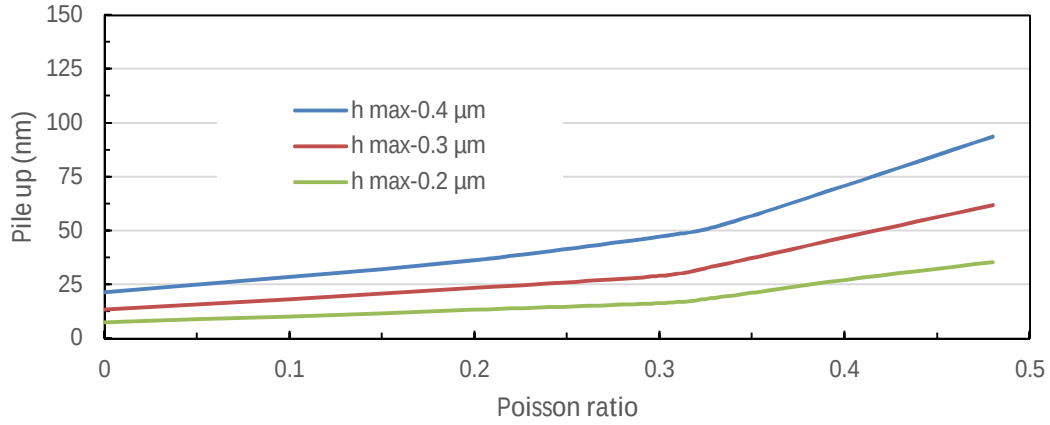

Fig. 4.40: Effect of Poisson ratio on maximum Pile up

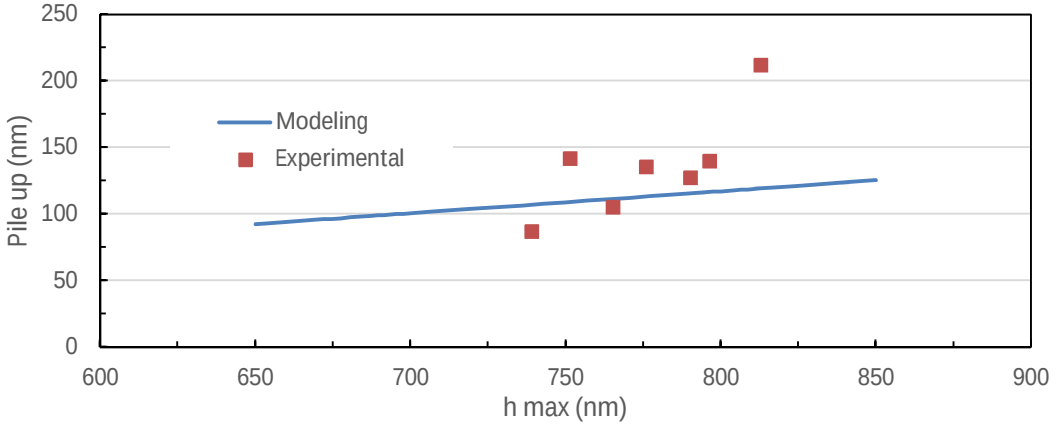

Fig. 4.41: Compare maximum Pile up corresponding Poisson ratio 0.33

The pile up curve with different depth corresponding to the Poisson ratio from 0 to 0.48 of Aluminum 6061 along the x-y plane to the specimen shown in Fig. 4.42, Fig. 4.43 and Fig. 4.44. The value of maximum pile up decreases with the decrease of indentation depth as well as the Poisson ratio.

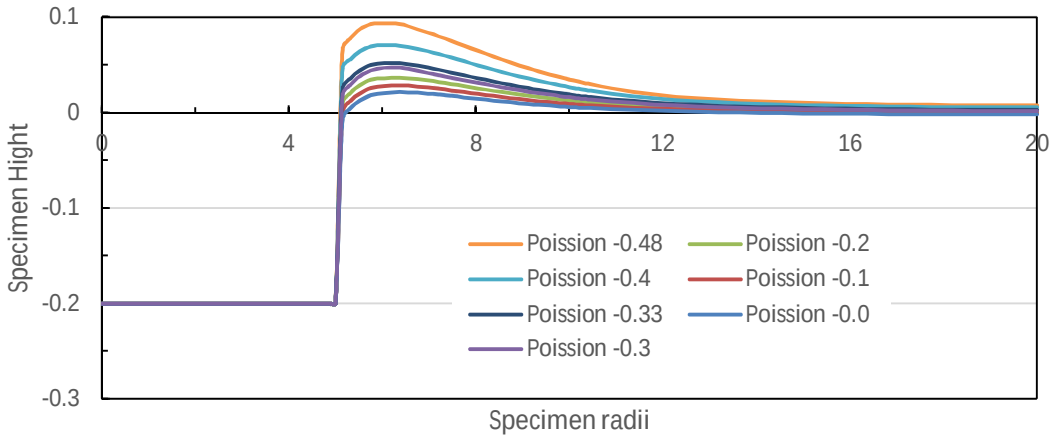

Fig. 4.42: Pile up curve corresponding to Poisson ratio with h_{max} 0.4 µm

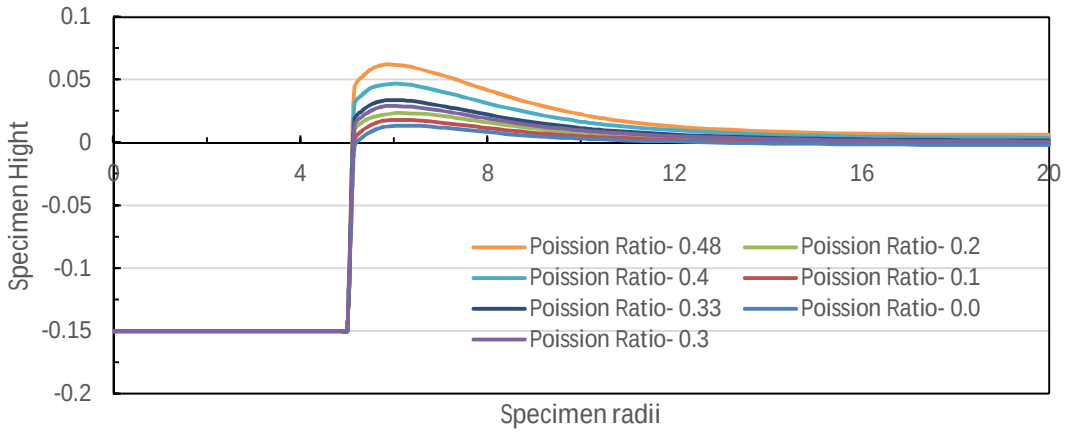

Fig. 4.43: Pile up curve corresponding to Poisson ratio with h_{max} 0.3 µm

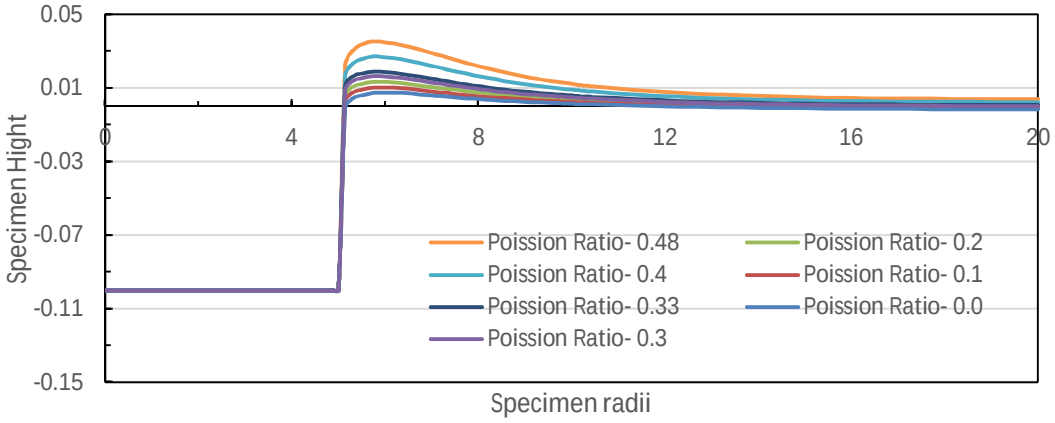

Fig. 4.44: Pile up curve corresponding to Poisson ratio with h_{max} 0.2 µm

4.5 Yield Strength and strain hardening

Yield strength is a vital parameter to characterize material's plastic properties by nanoindentation. Considering fully alignments of indenter, simulations were done for the different indentation material under the same strain hardening and the values for friction coefficient μ, strain hardening coefficient k and the exponential index m were figure out shown in Table 4.1. In practice, the yield point where the load is 73.9% of the elastic material model load is known as 0.1% yield offset based on modeling data and the 0.2% offset yield point is the point where the load is 68.6% the load of elastic material model. But the maximum indenting forces are comparatively incompatible because of the deviation between the yield strength and stress under the same strain.

Table 4.1: Computational value of k and m for different materials

	Elastic Modulus E (GPa)	Strain hardening coefficient, k	Exponential index, m
AISI-1018	208.242	500	0.315
AISI-4340	192.475	480	0.40
Aluminum 6061-T6	72.051	200	0.34

From the Fig. 4.45 it can be seen that the pile up slowly decreases with the increase of strain hardening index value corresponding to the maximum depth. The average experimental and modeling results is similar in the same Poisson ratio. Table 4.2 shows the maximum pile up data corresponding the index as varies Poisson ratio of three materials.

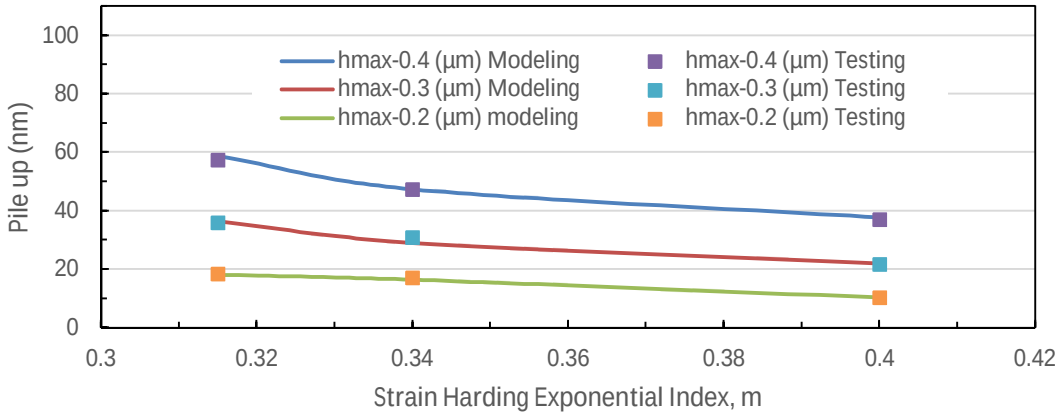

Fig. 4.45: Compare results of pile up vs exponential index in same Poisson ratio

Table 4.2: modeling data of pile up with respect of Poisson ratio

Materials	Poisson Ratio	Strain Harding Index	h_{max}-0.4(µm)	h_{max}-0.3 (µm)	h_{max}-0.2(µm)
			Pile up (um)		
AISI 1018	0	0.31	26.52	14.58	6.64
Al 6061		0.34	21.60	13.54	7.57
AISI 4340		0.40	15.59	7.70	2.72
AISI 1018	0.1	0.31	34.68	19.82	9.30
Al 6061		0.34	28.61	18.13	10.29
AISI 4340		0.40	22.41	12.17	5.08
AISI 1018	0.2	0.31	45.18	26.87	12.95
Al 6061		0.34	36.32	23.48	13.33
AISI 4340		0.4	29.97	17.97	8.14
AISI 1018	0.3	0.31	58.81	36.50	18.09
Al 6061		0.34	47.36	29.07	16.42
AISI 4340		0.40	37.67	21.96	10.34
AISI 1018	0.4	0.31	76.05	49.52	25.55
Al 6061		0.34	70.94	46.92	27.18
AISI 4340		0.40	49.43	26.92	14.43
AISI 1018	0.48	0.31	91.64	62.74	33.92
Al 6061		0.34	93.71	61.95	35.43
AISI 4340		0.40	65.03	36.63	18.62

Chapter 5 Conclusion

5.1 Concluding Assert

The current work indicate that, the cylindrical indentation technique can be used to characterize the elasticity and yield strength of the materials in nano scale where the conventional experimental mechanical tests become ineffectual or inaccessible. However, it is critical to reliably obtain these properties from the perspective of design and research. Indentation testing for Aluminum alloy 6061T6, low carbon steel AISI 1018 and alloy steel AISI4340 has been conducted by computer modeling and validated by experiments. The indentation modeling was done by constructing a 3-D symmetric model through ANSYS software considering Poisson ratio varies from 0 to 0.48 to extract the mechanical properties of materials.

During the simulation it was identified that the deformation under a cylindrical flat tip indenter with perfect alignment can quickly reach a steady state fully plastic flow and the indentation depth has very little effect on calculating the elastic modulus of the sample material as well as the modeling results. The model shows that the elastic modulus results from the unloading curve were less effect of Poisson ratio corresponding to the indentation depth. The hardness slowly increases with the increase of maximum indentation depth as well as increase the Poisson ratio and it was not influences of the mechanical properties.

From the modeling results the maximum pile up value for the three materials decreases with the decrease of Poisson ratio that was very sensitive. The maximum pile up value for Aluminum alloy 6061T6, low carbon steel AISI 1018 and alloy steel

AISI4340 is 47.36nm, 58.81nm and 37.67nm respectively when the Poisson ratio is 0.3. The modeling results were compared with corresponding experimental data in the same Poisson ratio where they were in good compatibility with each other.

In conclusion, computational approaches conducted in this study shows that the nano indentation with cylindrical flat tip is a unique and sophisticated tool for characterizing the elastic and plastic mechanics of materials in nano/micro scale.

5.2 Succeeding Progress

Typically FE simulations are more efficient and flexible to study the nanoindentation processes and thus to oblige progress in the analytical methods used for extracting mechanical properties from experimental data.

Current work is focused on the finite element modeling to study the elastic plastic properties of material by cylindrical flat punch indentation where major investigation lies on the effect of Poisson ratio over the mechanical properties of Aluminum alloy 6061T6, low carbon steel AISI 1018 and alloy steel AISI4340. To assist the current studies, ingenious methods can be introduced to characterize the mechanical properties on a significant tilted sample. The work can be extended by performing the Berkovich indenter or spherical indenter both simulation and the experimental test on the same material to validate the numerical findings as well as the proposed empirical model and geometrical corrections can be applied to compensate the effect of Poisson ratio on material properties.

In addition, the current numerical model can be refined to study some critical issues such as mesh distortion. Meshing the model might be responsible for remarkable errors in FEA study that effects the mechanical properties as the depth of indentation varies and calculating the exert pile up value. Moreover, new FEA simulation can be designed by re meshing which will help to understand the effect on the extracted parameters. The time saved may be used to conduct further sophisticated simulation with more elements in the particular surface that is important designing 3-D modeling of nanoindentation.

The transparent indenter could be used to perform the indentation test during experiments is another effective strategy. For this method an optics system can be embedded in the indenter so that the video image easily captured of the deformation of the specimen surface during indentation that recorded through the transparent indenter. It helps to measure the exert pile up shape during the practical testing by using of different microscopy and spectroscopy tools that will lead to the capability of providing simultaneous insights into the mechanics of several materials.

Chapter 6 Reference

[1] ASTM International, ASTM E132-04(2010), Standard Test Method for Poisson's Ratio at Room Temperature, West Conshohocken, Pennsylvania: American Society for Testing and Materials, 2010, p. 3.

[2] ASTM International, "ASTM E111-04(2010), Standard Test Method for Young's Modulus, Tangent Modulus, and Chord Modulus," American Society for Testing and Materials, 2010.

[3] L. Qian, M. Li, Z. Zhou, H. Yang and X. Shi, "Comparison of nano-indentation hardness to microhardness," *Surface and Coatings Technology*, vol. 195, no. 2-3, pp. 264-271, 2005.

[4] M. Doerner and W. Nix, "A Method for Interpreting the Data from Depth Sensing Indentation Instruments," *Journal of Materials Research,* vol. 01, no. 04, pp. 601-609, 1986.

[5] S. V. Hainsworth, H. W. Chandler and T. F. Page, "Analysis of nanoindentation load-displacement loading curves," *Journal of Materials Research,* vol. 11, no. 08, pp. 1987-1995, 1996.

[6] Y. P. Zheng, A. P. C. Choi, H. Y. Ling and Y. P. Huang, "Simultaneous estimation of Poisson's ratio and Young's modulus using a single indentation: a finite element study," *Measurement Science and Technology,* vol. 20, no. 04, p. 045706, 2009.

[7] J.-H. Kim, S.-C. Yeon, Y.-K. Jeon, J.-G. Kim and Y.-H. Kim, "Nano-indentation method for the measurement of the Poisson's ratio of MEMS thin films," *Sensors and Actuators A: Physical,* vol. 108, no. 1-3, pp. 20-27, 2003.

[8] S. Liu and Q. J. Wang, "Determination of Young's modulus and Poisson's ratio for coatings," *Surface and Coatings Technology,* vol. 201, no. 14, pp. 6470-6477, 2007.

[9] J. F. Cárdenas-García and J. Rasty, "The Indentation Test Revisited: Obtaining Poisson's Ratio," in *SEM X International Congress and Exposition on Experimental and Applied Mechanics*, Costa Mesa, California, 2004.

[10] C. A. Clifford and M. P. Seah, "Nanoindentation measurement of Young's modulus for compliant layers on stiffer substrates including the effect of Poisson's ratios," *Nanotechnology,* vol. 20, no. 14, p. 145708, 2009.

[11] C. A. Clifford and M. P. Seah, "Modelling of nanomechanical nanoindentation measurements using an AFM or nanoindenter for compliant layers on stiffer substrates," *Nanotechnology,* vol. 17, no. 21, pp. 5283-5292, 2006.

[12] W. Oliver and G. Pharr, "An improved technique for determining hardness and elastic modulus using load and displacement sensing indentation experiments," *Journal of materials research,* vol. 7, no. 6, pp. 1564-1583, 1992.

[13] B. B. Jung, S. H. Ko, H. K. Lee and H. C. Park, "Measurement of Young's Modulus and Poisson's Ratio of Thin Film by Combination of Bulge Test and Nano-Indentation," *AMR Advanced Materials Research,* Vols. 33-37, pp. 969-974, 2008.

[14] M. Bamber, K. Cooke, A. Mann and B. Derby, "Accurate determination of Young's modulus and Poisson's ratio of thin films by a combination of acoustic microscopy and nanoindentation," *Thin Solid Films*, Vols. 398-399, pp. 299-305, 2001.

[15] J. C. Hay, A. Bolshakov and G. M. Pharr, "A critical examination of the fundamental relations used in the analysis of nanoindentation data," *Journal of Materials Research,* vol. 14, no. 06, pp. 2296-2305, 1999.

[16] D.-H. Chen and H. Nisitani, "Effect of poisson's ratio on elastic-plastic stress under plane deformation," *Engineering Analysis with Boundary Elements,* vol. 20, no. 01, pp. 17-24, 1997.

[17] G. Pintaude, "Analysis of Spherical Contact Models for Differential Hardness as a Function of Poisson's Ratio," *J. Tribol Journal of Tribology,* vol. 137, no. 04, p. 044502, 2015.

[18] I. Green, "Poisson ratio effects and critical values in spherical and cylindrical Hertzian contacts," *Int. J. of Applied Mechanics and Engineering,* vol. 10, no. 03, pp. 451-462, 2005.

[19] J. Aw, H. Zhao, A. Norbury, L. Li, G. Rothwell and J. Ren, "Effects of Poisson's ratio on the deformation of thin membrane structures under indentation," *Physica Status Solidi (b),* vol. 252, no. 07, pp. 1526-1532, 2015.

[20] A. A. Abd-Elhady and H. E.-D. M. Sallam, "Effect of Poisson′s Ratio on Stress/Strain concentration at Circular Holes in Elastic Plates Subjected to Biaxial

Loading - Three Dimensional Finite Element Analysis," in *Characterization of Minerals, Metals, and Materials 2016,* Hoboken, NJ: John Wiley & Sons, Inc., 2016, pp. 43-55.

[21] P. Yu, W. Guo, C. She and J. Zhao, "The influence of Poisson's ratio on thickness-dependent stress concentration at elliptic holes in elastic plates," *International Journal of Fatigue,* vol. 30, no. 01, pp. 165-171, 2008.

[22] R. Grant, M. Lorenzo and J. Smart, "The effect of Poisson's ratio on stress concentrations," *The Journal of Strain Analysis for Engineering Design,* vol. 42, no. 02, pp. 95-104, 2007.

[23] Z. Abdulaliyev and S. Ataoglu, "Effect of Poisson's Ratio on Three-Dimensional Stress Distribution," *Journal of Applied Mechanics,* vol. 76, no. 01, p. 014506, 2009.

[24] J. Dundurs, "Dependence of stress on poisson's ratio in plane elasticity," *International Journal of Solids and Structures,* vol. 3, no. 6, pp. 1013-1021, 1967.

[25] E. Liu, G. Xiao, H. Wang, X. Yang and X. Shu, "Determination of the Poisson's ratio of viscoelastic materials based on the linear rheological model using instrumented indentation," *Soft Materials,* vol. 14, no. 01, pp. 38-45, 2015.

[26] G. E. Dieter and D. Bacon, Mechanical metallurgy, SI metric ed., London: McGraw-Hill, 1988.

[27] P. Ludwik, Elemente der technologischen Mechanik, Berlin: Springer, 1909.

[28] W.-S. Lee and T.-T. Su, "Mechanical properties and microstructural features of AISI 4340 high-strength alloy steel under quenched and tempered conditions," *Journal of Materials Processing Technology*, vol. 87, no. 1-3, pp. 198-206, 1999.

[29] A. C. Fischer-Cripps, Introduction to Contact Mechanics, 2nd ed., Springer US, 2007.

[30] W. C. Oliver and G. Pharr, "Measurement of hardness and elastic modulus by instrumented indentation: Advances in understanding and refinements to methodology," *Journal of materials research*, vol. 19, no. 1, pp. 3-20, 2004.

[31] J. Bressan, A. Tramontin and C. Rosa, "Modeling of nanoindentation of bulk and thin film by finite element method," *Wear*, vol. 258, no. 1-4, pp. 115-122, 2005.

[32] A. Bhattacharya and W. Nix, "Finite element simulation of indentation experiments," *International Journal of Solids and Structures*, vol. 24, no. 09, pp. 881-891, 1988.

[33] X. Huang, "Mechanical Characterization of Thin Film Materials with Nanoindentation Measurements and FE Analysis," *Journal of Composite Materials*, vol. 40, no. 15, pp. 1393-1407, 2005.

[34] N. Panich, "Nanoindentation of Silicon (100) Studied by Experimental and Finite Element Method," *KMUTT Research & Development Journal,* vol. 27, no. 3, pp. 273-284, 2004.

[35] N. Panich and S. Yong, "Improved method to determine the hardness and elastic moduli using nano-indentation," *KMITL Science Journal,* vol. 5, no. 2, pp. 483-492, 2005.

[36] H. Song, "Selected Mechanical Problems in Load and Depth Sensing Indentation Testing (PhD dissertation)," Rice University, Houston, USA, 1999.

[37] P. C. B. Poon, "A Critical Appraisal of Nonindnetation with Application to Elastic-plastic Solids and Soft Materials, (PhD dissertation)," California Institute of Technology, Pasadena, California, 2009.

[38] C. S. Rao and E. C. Reddy, "Finite element modeling of nanoindentation to extract load-displacement characteristics of bulk materials and thin films," *Indian Journal of Pure & Applied Physics,* vol. 47, no. 1, p. 54, 2009.

[39] F. Chen, R. Chang and L. Chen, "Determining the Plastic-Viscoplastic Mechanical Properties of Thin Films by Nanoindentation and Finite Element Method," Taipei, Taiwan, 2007, pp. 605-608.

[40] D. J. Strange and A. K. Varshneya, "Finite Element Simulation of Microindentation on Aluminum," *Journal of Materials Science,* vol. 36, no. 8, pp. 1943-1949, 2001.

[41] K. Gadelrab and . M. Chiesa, "Influence of nanoindenter tip radius on the estimation of the elastic modulus," pp. 03-47, 2011.

[42] ANSYS Inc., *ANSYS Theory Reference Manual,* ANSYS version 14.5, 2013.

[43] A. L. Yurkov , V. N. Skvortsov, I. A. Buyanovsky and R. M. Matvievsky, "Sliding friction of diamond on steel, sapphire, alumina and fused silica with and without lubricants," *Journal of Materials Science Letters,* vol. 16, no. 16, pp. 1370-1374, 1997.

[44] Z. Hu, K. Lynne and F. Delfanian, "Characterization of materials' elasticity and yield strength through micro-/nano-indentation testing with a cylindrical flat-tip indenter," *Journal of Materials Research,* vol. 30, no. 04, pp. 578-591, 2015.

[45] Z. Hu, K. J. Lynne, S. P. Markondapatnaikuni and F. Delfanian, "Material elastic–plastic property characterization by nanoindentation testing coupled with computer modeling," *Materials Science and Engineering: A,* vol. 587, pp. 268-282, 2013.

[46] J. Eldridge, D. Zhu and R. Miller, "Mesoscopic nonlinear elastic modulus of thermal barrier coatings determined by cylindrical punch indentation," *Journal of American Ceramic Society,* vol. 84, no. 11, pp. 2737-2739, 2001.

[47] M. Kashani, "Sources of Error in Relating Nanoindentation Results to Material Properties," Wichita State University, USA, (Ph.D. thesis), 2010.